PERTURBED ANGULAR CORRELATIONS - RARE EARTHS

PERTURBED ANGULAR CORRELATION STUDIES IN THE FERROMAGNETIC RARE EARTHS

By

THOMPSON ANDREW McMATH, B.Sc.

A Thesis

Submitted to the FAculty of Graduate Studies

in Partial Fulfilment of the Requirements

for the Degree

Master of Science

McMaster University

October 1967

MASTER OF SCIENCE
(Physics)

McMASTER UNIVERSITY
Hamilton, Ontario

TITLE: Perturbed Angular Correlation Studies in the Ferromagnetic Rare Earths.

AUTHOR: Thompson Andrew McMath, B.Sc. (Queen's University)

SUPERVISOR: Dr. J. A. Cameron

NUMBER OF PAGES: v, 67

SCOPE AND CONTENTS:

A low temperature apparatus has been constructed for the purpose of studying perturbed angular correlations in the ferromagnetic rare earth elements. The rotation of the 966.4 keV gamma vibrational state in ^{160}Dy was measured to be (1.61 ± 0.33) milliradians.

ACKNOWLEDGEMENTS

I should like to express my sincere appreciation to those who have made this research possible:

To Dr. J. A. Cameron for his constant interest in the work and many helpful suggestions;

To the members of the Perturbed Angular Correlation Group, Jim Murray, Walt Brooker and Mike Byrnes, for their cooperation in all phases of the experiment, and to Miss Candy Comeau, who did many of the drawings for this thesis;

To Jim Ungrin and the Beta Ray Spectroscopy Group for the use of their high resolution spectrometer;

To Mr . Bill Scott for his cooperation in providing liquid helium;

To Hamish Robertson for frequent advice on electronics;

To the Atom Beam Group for many stimulating lunch-time arguments and discussions, and the odd filched o-ring.

This research was supported by grants to the group by the National Research Council of Canada and the Alfred P. Sloan Foundation, and scholarships to the author from the National Research Council and the Government of the Province of Ontario.

TABLE OF CONTENTS

LIST OF FIGURES

CHAPTER I

INTRODUCTION

The study of perturbations in angular correlations has proven to be a useful tool for the investigation of properties of nuclei and the influence of nuclear surroundings. The angular correlation is perturbed by the interaction between internal or external electromagnetic fields and the nuclear electric and magnetic moments during the time interval between the formation and decay of the intermediate state of a nuclear decay. While this technique is most commonly used to determine the magnetic moments of excited nuclear states, it can also be used to study aspects of solid state physics, such as ferromagnetism.

The Perturbed Angular Correlation (PAC) Group at McMaster has primarily been interested in measuring g-values of vibrational band excited states of even-even isotopes. These measurements have been made for the most part at room temperature, using the internal field in iron, cobalt, or nickel as the perturbing agent. Six of the heavy rare earth metals, gadolinium, terbium, dysprosium, holmium, erbium, and thulium, also become ferromagnetic at low temperatures, and their internal fields, with the exception of gadolinium, are an order of magnitude larger

than those of the iron group. Hence, nuclear states with lifetimes a factor of ten shorter can be studied in these fields. To take advantage of this situation, a low temperature apparatus incorporating a small superconducting magnet has been built; this will be described in detail in Chapter III.

The rare earth elements form one of the most interesting groups of the periodic table. These elements, from lanthanum to lutetium, and also the actinides, differ very slightly in their chemical properties; no other series of elements displays such small, uniform changes. They are very difficult to separate chemically and as a result of this, high purity samples have become available only recently.

The reason for this small variation in properties can be traced to the electronic structure. With increasing atomic number, the additional electrons fill the 4f shell; however, these states only become energetically favourable after the 4d, 5s, 5p and 6s shells have been filled, and one electron has been placed in a 5d state. The 4f shell, however, is deeply buried within the atom; its radius varies from 35% (La) to 20% (Lu) of the atomic radius. Thus the shell which determines the difference in properties only participates to a small degree in determining the overall atomic properties.

The rare earths crystallize in close-packed structure, with the exception of europium which is b.c.c. The ferromagnetic rare earths all form hexagonal close pack crystals, with c/a ratios between 1.59 and 1.57, quite close to the ideal value of 1.633. According to Gschneider (1961), the rare earths should alloy with each other quite easily, again with the exception of europium; this point is very important for the preparation of sources.

The first experiment performed on the adapted apparatus was a measurement of the rotation of the 2 + 966 keV gamma vibrational state of ^{160}Dy.

CHAPTER II

THEORY

1. Angular Correlations

In sections 1 and 2, no attempt has been made to provide a rigorous development of the theory of angular correlations. For full detail , refer to the articles by Steffen and Frauenfelder.

The probability of emission of a particle or quantum by a decaying nucleus depends generally on the angle between the nuclear spin and the direction of emission. Because of the random orientation of nuclei, the observed radiation from an active source is isotropic under ordinary circumstances. If, however, the nuclei have some non-random distribution of orientations, an anisotropic pattern may be observed. Such a non-random array can be realized in several ways. A strong magnetic field or electric field gradient can be used to align the nuclei. Another approach is to select only those nuclei whose spins happen to lie in some preferred direction. If a nucleus decays by a cascade of radiations, the observation of one radiation in some fixed direction implies a non-random distribution of possible orientations of the nucleus from which it was emitted; successive radiation may then have a definite

angular correlation with respect to the direction of the first emission.

If in its decay a nucleus emits two gamma rays γ_1 and γ_2 in directions $\vec{k}_1$ and $\vec{k}_2$ in rapid succession, the relative probability that γ_2 is emitted into a solid angle $d\Omega$ at angle θ with respect to k_1 is expressed as $W(\theta)d\Omega$. If γ_1 is a pure transition between nuclear states I_i, m_i and I, m, then γ_1 is characterized by the angular momentum quantum number L_1 and the magnetic quantum number M_1. To conserve angular momentum, we have $\vec{I}_i = \vec{I} + \vec{L}_1$; similarly $m_i = m + M_1$.

Each component $m_i \rightarrow m$ between specific magnetic sublevels has a characteristic directional distribution $F_{L_1}^{M_1}(\phi)$ with respect to the quantization axis which is independent of I_i and I; these distributions can be calculated from the Poynting vector expressed as a function of angle, for multipole radiation characterized by L and M. Since for gamma rays the different M components are not separated, the directional distribution $F_{L_1}(\phi)$ of the unresolved line is given by

$$F_{L_1}(\phi) \alpha \sum_{m_i m} P(m_i)\ G(m_i m)\ F_{L_1}^{M_1}(\phi)$$

where $P(m_i)$ is the relative population of sublevel m_i

and $G(m_i m) = \langle I m L_1 M_1 | I_i m_i \rangle^2$ is the relative transition probability for component $m_i \rightarrow m$. If the nuclei are randomly oriented, all the m_i states are equally populated, and the distribution $F_{L_1}(\emptyset)$ is isotropic.

For physical reasons, the distribution $W(\theta)$ must be independent of the choice of z axis. If the z axis is taken parallel to $\vec{k}_1$, then $W(\theta)$ becomes identical with the directional distribution $F_{L_2}(\emptyset)$ of γ_2 with respect to the quantization axis. This can be calculated once the relative populations $P(m)$ of the intermediate state are known. Assuming all the m_i states are equally populated,

$$P(m) \alpha \sum_{m_i} G(m_i m) F_{L_1}^{M_1}(0).$$

However, a photon can only carry angular momentum of $\pm \hbar$, and since γ_1 travels along the z-axis, M_1 is restricted to the values ± 1. Thus the states $P(m)$ are not equally populated, and a directional correlation results:

$$W(\theta) \alpha \sum_{m_i m m_f} \langle I m L_1 \pm 1 | I_i m_i \rangle^2 F_{L_1}^{\pm 1}(0) \langle I_f m_f L_2 M_2 | I m \rangle^2 F_{L_2}^{M_2}(\theta) .$$

A more rigorous development must be followed to allow for transitions of mixed multipolarity.

The eigenfunctions of radiation emitted in direction $\vec{k}$ with spin $\vec{\sigma}$ can be denoted as $\langle k\sigma | LM\pi \rangle$, defined in terms of the nuclear properties L, M, π, with respect to an arbitrary quantization axis. As above, simplification arises if the

z-axis coincides with $\vec{k}$. In this case, the eigenfunctions are denoted as $\langle O\sigma|L\mu\pi\rangle$, and correspond to a plane wave propagating along the direction of emission, i.e. to emission with intrinsic angular momentum only. These simpler eigenfunctions can be defined for both γ_1 and γ_2, each in its own coordinate system. The eigenfunctions in the two systems are related by

$$\langle k\sigma|LM\pi\rangle = \sum_{\mu} \langle O\sigma|L\mu\pi\rangle \, D^{L}_{\mu M} \, (k \to z) \ , \qquad (1)$$

where $D^{L}_{\mu M}$ $(k \to z)$ are the elements of the rotation matrix which carries the coordinate system of the radiation over into the arbitrary quantization system.

The directional correlation function can be written

$$W(k_1,k_2) = S_1 S_2 \sum_{m_f m m' m_i} \langle m_f|H_2|m\rangle\langle m|H_1|m_i\rangle\langle m'|H_1|m_i\rangle^{*}\langle m_f|H_2|m'\rangle^{*} \qquad (2)$$

where S_1 and S_2 indicate summation over all unmeasured radiation properties of γ_1 and γ_2 such as spin and polarization, and H_1 is the interaction operator for the emission of γ_1 in direction $\vec{k}_1$ with polarization $\vec{\sigma}_1$. The matrix elements $\langle m|H|m_i\rangle \equiv \langle Imk\sigma|H|I_i m_i\rangle$ can be expressed as

$$\sum_{LM\pi} \langle k\sigma|LM\pi\rangle\langle ImLM\pi|H|I_i m_i\rangle \ .$$

The first part of this can be expressed in terms of the simpler eigenfunctions in the coordinate system of the radiation as in (1) and the m dependence can be removed from the second part using the Wigner-Eckart theorem.

If only the directions and not the polarizations of the two radiations are observed, the combined expression above can be stated in a very concise form. The representations D^L become Legendre polynomials, and the directional correlation simplifies to

$$W(\theta) = \sum_{k \text{ even}} A_{kk} P_k (\cos \theta).$$

The coefficients A_{kk} in this expansion can be broken into independent factors for the two transitions of the cascade: $A_{kk} = A_k(1) A_k(2)$, where the terms $A_k(j)$ contain the spin coupling and radiation parameters and the reduced matrix elements.

This can be written in the equivalent form

$$W(\theta) = \sum_n B_{2n} \cos(2n\theta)$$

which may be easier to handle analytically under certain conditions.

2. Perturbed Angular Correlations

A cascade $I_i \rightarrow I \rightarrow I_f$ can no longer be described by (2) if during its intermediate state I it is subjected to a torque, due to the interaction of either the magnetic moment μ with an extranuclear magnetic field H or of the electric quadrupole moment Q with an electric field gradient $\frac{\partial^2 V}{\partial z^2}$, since the final states $\langle m_a|$ and $\langle m_a'|$ after emission of the first radiation are no longer identical to the initial states $|m_b\rangle$ and $|m_b'\rangle$ of the second radiation. The change

from state $|m_a>$ to state $|m_b>$ induced by an extranuclear field can be described by an evolution operator $\Lambda(t)$:

$$|m_b> = \Lambda(t)\,|m_a> \ .$$

This operator must satisfy the Schrodinger equation

$$\frac{\partial}{\partial t}\,\Lambda(t) = -\frac{i}{\hbar}\,K\cdot\Lambda(t)$$

where K is the Hamiltonian describing the interaction. For static interactions the solution is

$$\Lambda(t) = \exp\,[-\frac{i}{\hbar}\,K\,t].$$

The directional correlation may now be described by

$$W(k_1,k_2,t) = \sum_{(m_f m_b m_b' m_a m_a' m_i)} <m_f|H_2|m_b><m_b|\Lambda(t)|m_a> \times <m_a|H_1|m_i><m_f|H_2|m_b'>^{*}<m_b'|\Lambda(t)|m_a'>^{*}<m_a'|H_1|m_i>^{*} \quad (3)$$

where t is the time of emission of γ_2 following the emission of γ_1 at t = 0.

The Hamiltonian describing the interaction between the nuclear magnetic moment μ of the intermediate state and a magnetic field H, which we take in the direction of the positive z-axis, is $K_H = -\vec{\mu}\cdot\vec{H} = -\mu_z H$. The matrix elements of K are $<Im|K_H|Im'> = -H\,<Im|\mu_z|Im'>$, and since $\mu_z = \gamma I_z$ the matrix is diagonal. The energy eigenvalues are $E_m = -\frac{\mu H m}{I} = m\hbar\omega$, where ω is the Larmor frequency, defined by

$$\omega = \frac{(E_{m+1} - E_m)}{\hbar} = -\frac{g\mu_N H}{\hbar}$$

Here g is the g-value of the intermediate state and μ_N is the nuclear magneton. The matrix element of the evolution operator $\langle m_b | \Lambda(t) | m_a \rangle$ in (3) is thus proportional to $\exp [-i (m_b - m_a) \omega t]$.

The interaction causes a precession of the nucleus about the field direction at frequency ω, which effectively rotates the angular correlation pattern by an angle ωt. The angular correlation function is particularly simple if the two radiations are viewed in a plane perpendicular to the direction of the magnetic field. The rotated correlation pattern is then given by

$$W \quad (\theta, H, t) = \sum_n B_{2n} \cos 2n(\theta - \omega t). \qquad (4)$$

The interaction between an electrostatic gradient and the electric quadrupole moment of the intermediate state is described by the Hamiltonian

$$K_Q = \sum_q \frac{4}{5}\pi (-1)^q T_q^{(2)} V_q^{(2)}$$

where $T^{(2)}$ and $V^{(2)}$ are tensor operators of the nuclear quadrupole moment and the classical external field gradient. The conventional definition of the electric quadrupole moment Q is

$$eQ = 4\sqrt{\frac{\pi}{5}} \langle II | T_o^{(2)} | II \rangle.$$

The elements of the (diagonal) interaction matrix elements are

$$\langle Im|K_Q|Im\rangle = E_m = \frac{3m^2 - I(I+1)}{4I(2I-1)} e Q V_{zz} .$$

These may also be expressed in terms of the quadrupole frequency $\omega_Q = -\frac{e Q V_{zz}}{4I(2I-1)\hbar}$. The energy eigenvalues are doubly degenerate , since they depend on m^2, and the quadrupole rotations are insensitive to the direction of a magnetic field. Thus in an experiment in which a magnetic field is used as the perturbing agent, quadrupole effects will be limited to attenuations.

3. Measurement of the Rotation

The expressions developed above give the time differential perturbed angular correlation, i.e. the correlation measured if γ_2 is observed within the time interval from t to t + dt after the emission of γ_1. In an actual experiment where the resolving time of the apparatus is much longer than the mean life τ of the intermediate state, the time-integrated correlation is observed:

$$W(\Theta ,H,\infty) = \frac{1}{\tau} \int_0^\infty e^{-\frac{t}{\tau}} W(\theta,H,t)\, dt.$$

This will be denoted as $W(\theta,H)$. Substituting expression (4) in this equation gives

$$W(\theta,H) = \sum_n \frac{B_{2n}}{1+(2n\omega\tau)^2} (\cos 2n\theta + 2n\omega\tau \sin 2n\theta)$$

The rotation of the angular correlation pattern in a magnetic field is observed by first determining the zero field pattern, then measuring the coincidence rates at some

fixed angle θ' with field "up" and field "down". The direction of the rotation $\omega\tau$ depends on the direction of the field;with the field in one direction the rotation is such that the coincidence rate at θ' is increased from the zero field case, but when the field is reversed, the coincidence rate is decreased. θ' is chosen to maximize the difference. The experimentally determined parameter is

$$\frac{R}{2} = \frac{W(\theta',H) - W(\theta',-H)}{W(\theta',H) + W(\theta',-H)}$$

$$= \frac{\sum_n \frac{B_{2n}}{1+(2n\omega\tau)^2} 2n\omega\tau \sin 2n\theta'}{\sum_n \frac{B_{2n}}{1+(2n\omega\tau)^2} \cos 2n\theta'}$$

If the rotation $\omega\tau$ is small, this can be approximated by

$$\frac{R}{2} = -\left[\frac{1}{W(\theta)} \frac{dW(\theta)}{d\theta}\right]_{\theta'} \frac{g\mu_N H}{\hbar} \tau \quad .$$

Note that the rotation is determined by three factors: the mean life τ of the intermediate state, the g-value of the intermediate state, and the field H at the nucleus. If any two of these factors are known, the third can be determined.

4. Effective Field at the Nucleus

Early perturbed angular correlation measurements were done using external fields, and it was usually necessary to work with states whose lifetimes are greater than 10^{-10} seconds. To study shorter lived states, it is necessary to use the hyperfine field as the perturbing agent; the nuclei

are alloyed as an impurity in a ferromagnetic host, which is then magnetically saturated.

According to Marshall (1961) the effective magnetic field at the nucleus can be written as

$$H_{eff} = H_{\ell} + H_c + H_a$$

where H_{ℓ} is the local magnetic field at the position of the nucleus,

H_c is the effective magnetic field due to the contact interaction with the s-electrons,

H_a is the effective magnetic field due to the interactions of the nucleus with electrons on the same atom.

The local magnetic field H_{ℓ} includes the external field, the Lorentz field, and the demagnetizing field which depends only on the shape of the sample.

The contact field H_c, which is nonzero only for s electrons, may be regarded as the sum of two parts. The first part is proportional to the conduction electron polarization. The density at the nucleus of an unpaired outer s-electron was first treated by Fermi in his study of hyperfine fields in free atoms, and was historically considered responsible for the observed magnetic field. If there are no unpaired s-electrons but a net spin exists, the core electrons can be polarized by the spin of the outer electrons to create a net spin density at the nucleus. The second term in H_c comes from configuration mixing of the s-electrons

into the unfilled electron band.

The effective field H_a is comprised of several terms. These include the contact interaction with the inner s-electrons; the dipole-dipole interaction between nuclear and electron spins, the interaction between the nucleus and the unquenched part of the orbital moment; and cross terms between the dipole-dipole interaction and spin-orbit coupling.

In the 3d transition elements, core polarization and conduction electron polarization provide the strongest contributions to the effective field. These give rise to fields of the order of several hundred kilogauss. In the rare earths the dominant effects, according to Kondo (1961) and Watson and Freeman (1961) are caused by the orbital angular momentum of the unfilled 4f shell, and to a lesser extent, the spin exchange polarization of core and conduction electrons. The orbital angular momentum of the 4f shell is almost completely unquenched in the rare earths, and produces a field of several thousand kilogauss. Gadolinium and europium, which have half filled electron shells, are exceptions to this; the main contribution in these cases comes from core polarization, and the fields are relatively small. Some values of effective fields in rare earths are shown in table II-1.

TABLE II-1

Effective fields at the nucleus of the rare earths

Element	Z	No. 4f electrons	H_{eff} (kilogauss)		
Pr	59	2	3600		
Nd	60	3	4200		
Sm	62	5	3300	3300	SH
Eu	63	7		267	NMR
Gd	64	7		340	PNR
Tb	65	8	4200	3600	NMR
Dy	66	9	7300	6500	NMR
Ho	67	10	9000	9300	SH
Er	68	11	9000		
Tm	69	12	7900	6960	Mo
Yb	70	14	4200		

Note: The values of H_{eff} in the first column were calculated (Kondo 1961); the values in the second column were determined experimentally by the methods indicated

NMR nuclear magnetic resonance

SH specific heat

PNR polarized neutron resonance

Mo Mossbauer effect

Some discrepancies may arise from the use of different ground state moments.

Using the enormous internal fields of the ferromagnetic rare earths, states with lifetimes of the order of 10^{-12} seconds can be studied with perturbed angular correlations. Since the effective field is mainly dependent on the deeply-buried 4f shell, it might be expected that the field at the nucleus of an impurity atom in a dilute alloy of rare earths will depend more on the impurity atom itself than on the host element.

5. Magnetism in the Rare Earths

The six ferromagnetic rare earth elements display a wide variety of magnetic structures (Koehler, 1965, and Yosida). Only gadolinium is a simple ferromagnet, with a Curie temperature of 290°K. The structures of the remaining elements can be regarded as deformed screw structures, which may be described as follows.

The general expression for the anisotropy of crystals of hexagonal symmetry is given by

$$\mathcal{H} = K_2^o P_2 (\cos\theta) + K_4^o P_4 (\cos\theta) + K_6^o P_6 (\cos\theta)$$

$$+ K_6^6 \sin^6\theta \cos 6\phi$$

where θ and ϕ are the angles of moments with respect to the c and a axes (see Fig. II-1). The anisotropy constants K_ℓ^m include contributions from both single ion and exchange interactions.

Fig. II-1. A magnetic screw structure, typical of those found in the ferromagnetic rare earths. The magnetic moments in any c plane are parallel, but the c plane projections of the moments of atoms in adjacent planes are displaced by an angle ϕ .

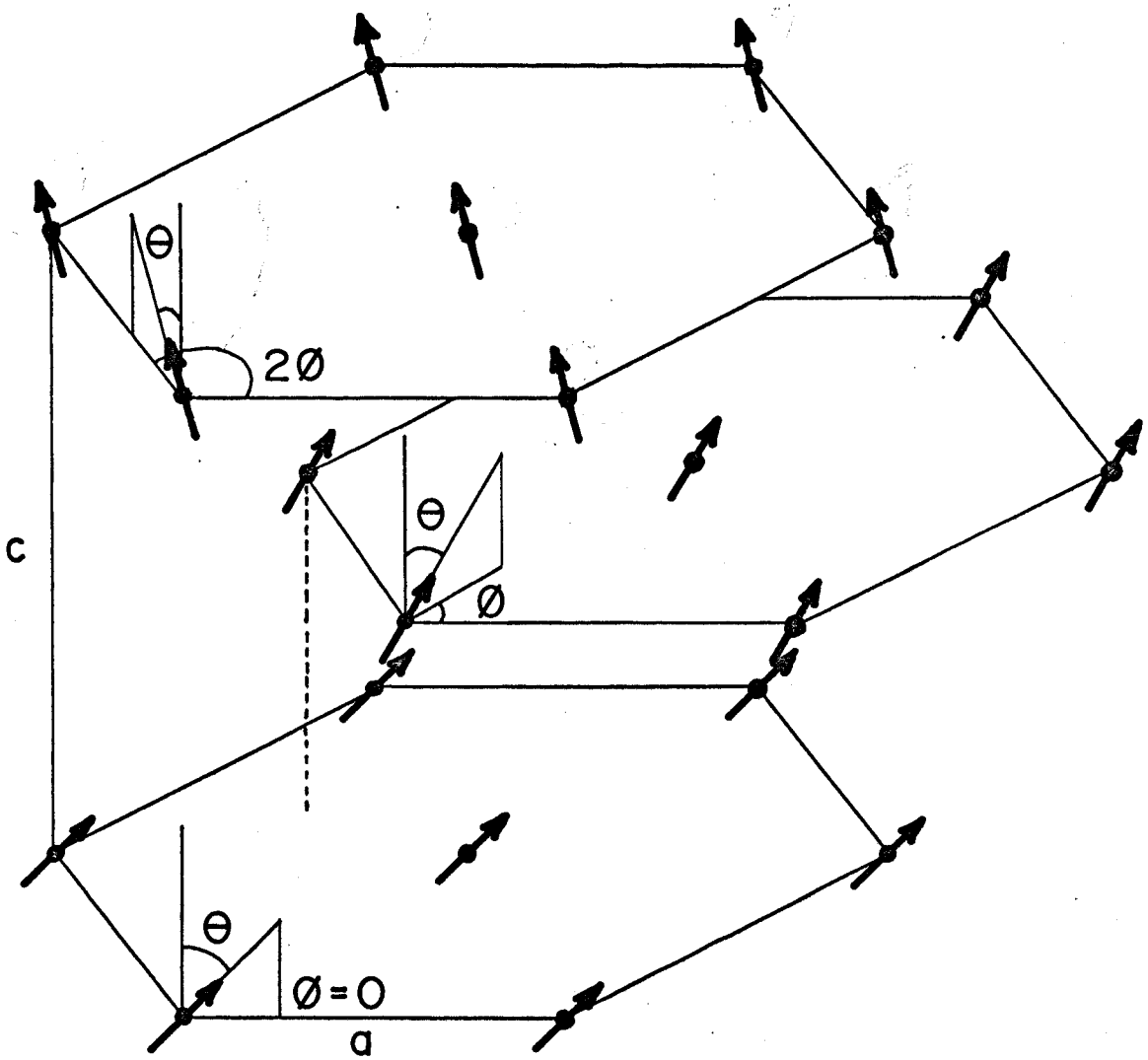
θ
2Ø
θ
Ø
c
θ
Ø=0
a

Terbium and dysprosium have similar magnetic structures. In both, the c axis is very hard magnetically, and the magnetic moments are confined to the c planes (i.e. $\Theta = 90^{o}$). Both pass through an antiferromagnetic screw phase, in which all the moments in one plane are aligned but the moments in adjacent planes are displaced by a definite angle $\emptyset$; this is the proper screw structure. They become ferromagnetic (in the c planes) at $218^{o}K$ (terbium) and $87^{o}K$ (dysprosium). The anisotropy coefficients in units of ergs per cm^3 for terbium are $K_2^{o} = 5.5 \times 10^8$ and $K_6^{6} = 2.4 \times 10^6$ at $4^{o}K$, and for dysprosium, $K_2^{o} = 5 \times 10^8$ ($20^{o}K$) and $K_6^{6} = 7.5 \times 10^6$ ($4^{o}K$) (Rhyne and Clark, 1967). Note that the base plane anisotropy coefficients are of the same order of magnitude as the cubic anisotropy coefficients of cobalt, and slightly larger than those of iron.

Holmium displays a screw structure in the base plane below $133^{o}K$, and below the Curie temperature of $19^{o}K$ a net component forms along the c axis, resulting in a conical screw structure. The structure of erbium is even more complicated; below $20^{o}K$ it has a conical screw structure similar to that of holmium, and above the Curie point it passes through two antiferromagnetic phases, with moments sinusoidally oscillating both along the c axis and in the c plane, and at higher temperatures, oscillating along the c axis only. The c plane is magnetically hard in thulium, and

moments align along the c axis with amplitudes sinusoidally varying at higher temperatures; below 38°K the moments lie in antiphase, with four pointing "up" to every three pointing "down".

Ruderman and Kittel (1954) proposed an indirect exchange between two nuclei via the conduction electrons to account for the anomalous broadening of NMR lines. The interaction between nuclei via the double scattering of an electron ($k \to k' \to k$) can be expressed

$$\mathcal{H}(R_{ij}) = -(\vec{s}\cdot\vec{I}_i)(\vec{s}\cdot\vec{I}_j) \int_0^{k_m} \frac{dk}{(2\pi)^3} \int_{k_m}^{\infty} \frac{dk'}{(2\pi)^3} \frac{\exp[i(\vec{k}-\vec{k}')\cdot R_{ij}]}{E(k')-E(k)} + c.c.$$

This has a solution of the form

$$\frac{\vec{I}_i\cdot\vec{I}_j}{R_{ij}^4}\,[2kR_{ij}\cos(2kR_{ij}) - \sin(2kR_{ij})]\ .$$

Kasuya (1956) and Yosida (1957) pointed out that a long range oscillatory interaction with a minimum fourier transform at nonzero q was required to stabilize magnetic structures of the type outlined above, and suggested that the Ruderman-Kittel interaction was dominant in the rare earths.

One possible explanation for the different behaviour of gadolinium is that with decreasing nuclear charge, the radius of the 4f shell increases with respect to the lattice constant, and the direct exchange interaction may become appreciable. Since gadolinium has a half filled 4f shell,

the orbital angular momentum term is identically zero.

Behrendt, Legvold, and Spedding (1958) and Hegland, Legvold and Spedding (1963) show that the easy direction of magnetization in the base plane is the (a) direction $\langle 11\bar{2}0\rangle$ in dysprosium, and the (b) direction $\langle 10\bar{1}0\rangle$ in terbium. In both cases, magnetization along the easy direction reaches saturation at a fairly low field, whereas the magnetization curve for the harder direction retains a small positive slope at relatively high fields. From this and from the magnitudes involved, it appears that the moments align along the closest easy direction, and that initially the magnetization seen along the hard directions is due to the projection of the moments on the hard directions.

The magnetization in a metal sample for small applied fields can be obtained if we assume that the moments will align with the easy direction in the base plane which is closest to the applied field, and that the magnetization seen will be due to the projection of the moments on the direction of the applied field; then, integrating over all orientations of the base plane and over the possible directions of easy magnetization in the base plane, we obtain $M_{metal} = \frac{3}{4} M$ easy direction.

CHAPTER III

APPARATUS

1. General

The low temperature system has been designed as an extension of the apparatus of the perturbed angular correlations group. There are two reasons motivating the construction of a low temperature apparatus: first, the heavy rare earth elements become ferromagnetic only at low temperatures, with Curie points ranging from 289 ^{o}K (Gd) to 20 ^{o}K (Ho and Er); second, the magnetic field produced by even a small superconducting magnet is considerably larger than the 2 kilogauss maximum field of the older magnet. This is an important consideration as the rare earths are magnetically hard.

The system was designed to utilize fully the previously existing data collection system. A photograph of the apparatus is shown, with the dewar vessels and detectors mounted for an experiment, in Figure III-1.

2. Cryostat

The superconducting magnet is mounted inside a pair of glass dewars, as shown in Figure III-2. Both dewars are silvered on the inner surfaces of their vacuum jackets, to minimize radiation heating; both have a thin unsilvered vertical strip to permit viewing of the

Fig.III-1. The low temperature perturbed angular correlation apparatus.

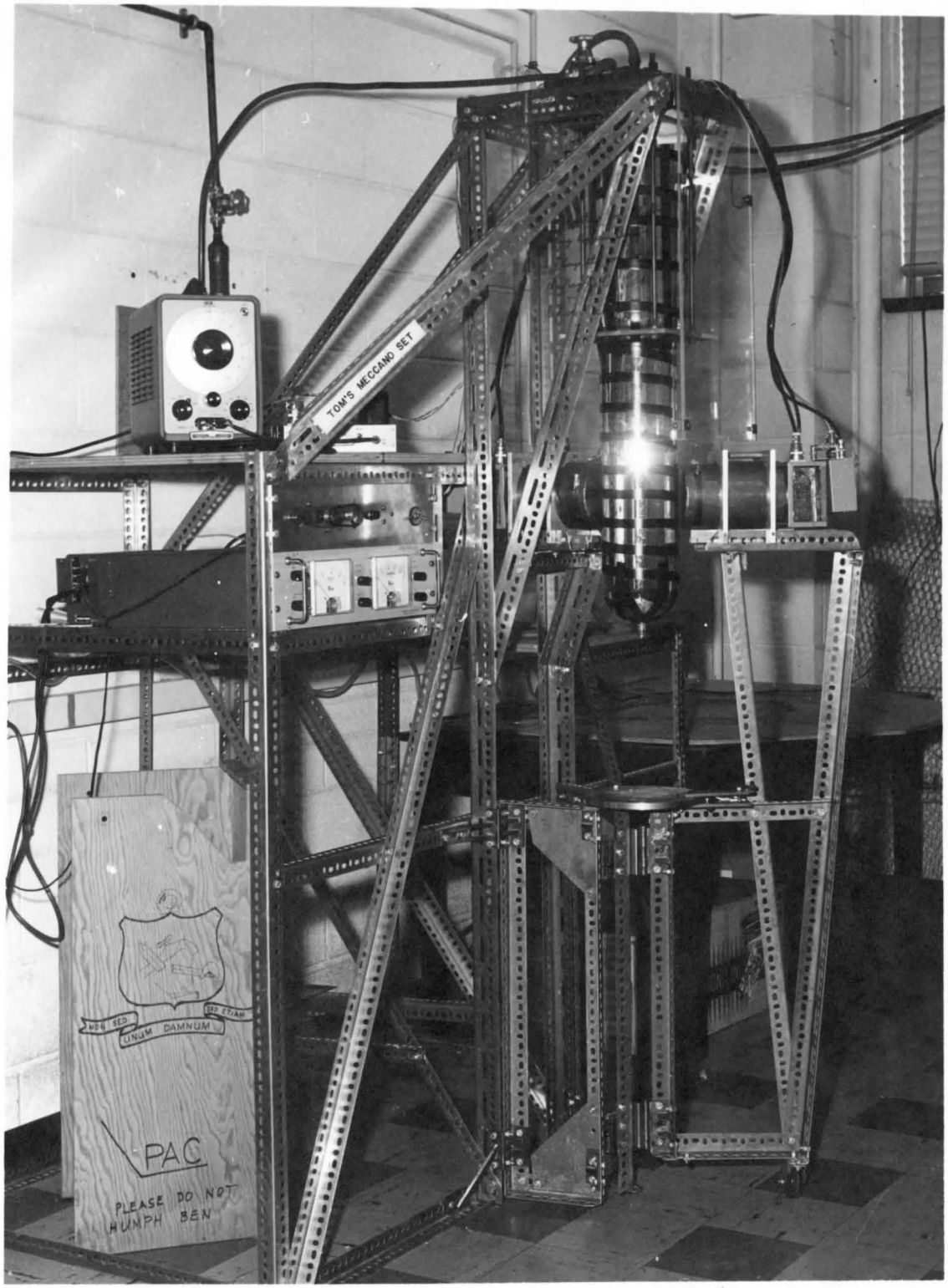
TOM'S MECCANO SET
PAC
PLEASE DO NOT
HUMPH BEN

Fig. III-2. The liquid helium cryostat and magnet.

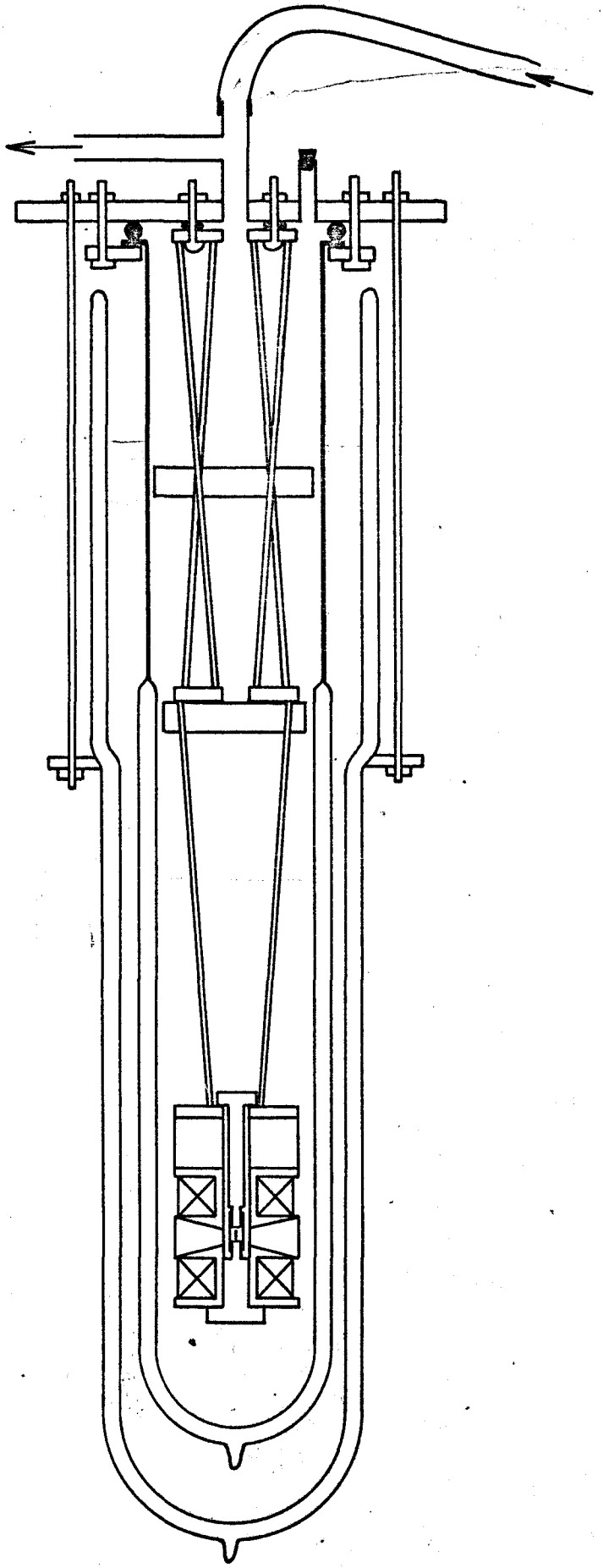

liquid levels. The inner dewar holds approximately three liters of liquid helium, or about two liters above the top of the magnet.

The cryostat was designed to keep heat leaks into the liquid helium to a minimum. The main current leads represent a compromise between small cross-section, to minimize heat conduction, and large cross-section, to minimize ohmic heating. Three strands of 30 gauge wire in each lead carry the current through the liquid helium to and from the magnet; this is increased to four strands apiece above the highest liquid helium level, and again to six strands near the top of the cryostat. Outside the cryostat, the current is carried by a single strand of 12 gauge wire; multiple strands are used inside to increase the surface area of the conductor and give more efficient cooling. Other leads, down to the depth indicator and saturation testing coils (to be described later) are single strands of #36 gauge wire.

The magnet itself is supported by three thin-walled stainless steel tubes. To increase the rigidity of the support, these are soldered to a brass plate, which is rigidly supported from the top plate by six more stainless steel tubes, arranged in three X's at 120^{o} to each other. This is shown in Figure III-2.

As a final precaution against heat leaks, two styrofoam baffles are placed across the neck of the dewar

to prevent radiation downwards from the top plate. The helium boil-off rate was observed to range from 0.25 litres per hour with the helium dewar almost full, to 0.1 liters per hour with the helium level just above the top of the magnet; these measurements were made with a magnet current of ten amperes.

The helium gas which is boiled off in the cryostat is returned to the helium liquifier in the Senior Science Building via an underground pipe. To prevent air from contaminating the helium, the entire system has been made leakproof. O-ring seals are placed between the helium dewar and the top plate, and around each of the bolts holding the magnet support to the top plate. Power and signal leads are brought through the top plate by means of hermetically sealed feed-through connectors. The tube for the helium transfer siphon is kept tightly sealed with a rubber stopper.

Helium gas boiling off from the 25 liter helium storage vessel is also transferred into the return line by means of the gum rubber tube fastened to the tee mounted on the top plate (ref. fig. III-2). This tee is located directly above the center of the magnet, and each of the brass plates in the magnet support has a central 1/2 inch diameter hole; this is to permit a future modification to allow sources to be mounted in the magnet without completely

disassembling the dewar system.

One of the detectors is mounted permanently between the uprights of the support frame; the other is mounted on a swinging gate, which pivots about a point directly below the center of the magnet. The pivot is not rigidly fixed to the main frame, however, as this would prevent the removal of the dewars. Two small gates swing from the main uprights of the support frame, and are locked together by two sliding bolts to form a rigid base from which the detector gate swings. These gates are unlocked and swung aside when the dewars are being mounted or removed. A disc, scribed every ten degrees of arc, is fixed to one of these small gates, and a pointer on the detector gate then indicates the angle between the fixed detector and the moving detector. The detector gate can be clamped to this disc once the proper angle has been selected. The length of the arms of the two small gates can be altered to align the detector gate pivot with the center of the magnet; this was done using a plumb bob.

3. Magnet

A photograph of the magnet and the two detectors is shown in Figure III-4; the detectors are in the positions they would occupy with the dewars up during an experiment.

The magnet was custom made by Oxford Instrument Co. Ltd. It features a split coil arrangement, with two

30^{o} wedge coil spacers, to permit clear passage for radiation over a large range of angles in the horizontal plane. A maximum field of 16.7 kG is produced, corresponding to a current of 19 amps.

The magnet is powered by a Harrison Laboratories 6264A power supply, capable of producing 20 amperes at 18 volts. The power supply is operated in a constant current resistance programmed mode. A high quality ten-turn variable resistor is used as the reference resistance. To change the current output, the resistance is increased or decreased by means of a small reversible motor. The current leads pass through a reversing switch, which controls the field direction. Both the field reversing switch and the switch controlling the reference-resistance motor are hand operated.

Two diodes in parallel with the magnet provide a bypass which carries the current if the magnet becomes normal. Since they have higher impedance than the magnet, the diodes are not usually conducting.

The system is shown schematically in Figure III-3.

4. Saturation Testing Transformer

It is vital to know when the sample is being magnetically saturated. A device to test saturation by measuring the incremental susceptibility of the sample has been incorporated in the source holder.

Fig. III-3. A schematic of the magnet field control system.

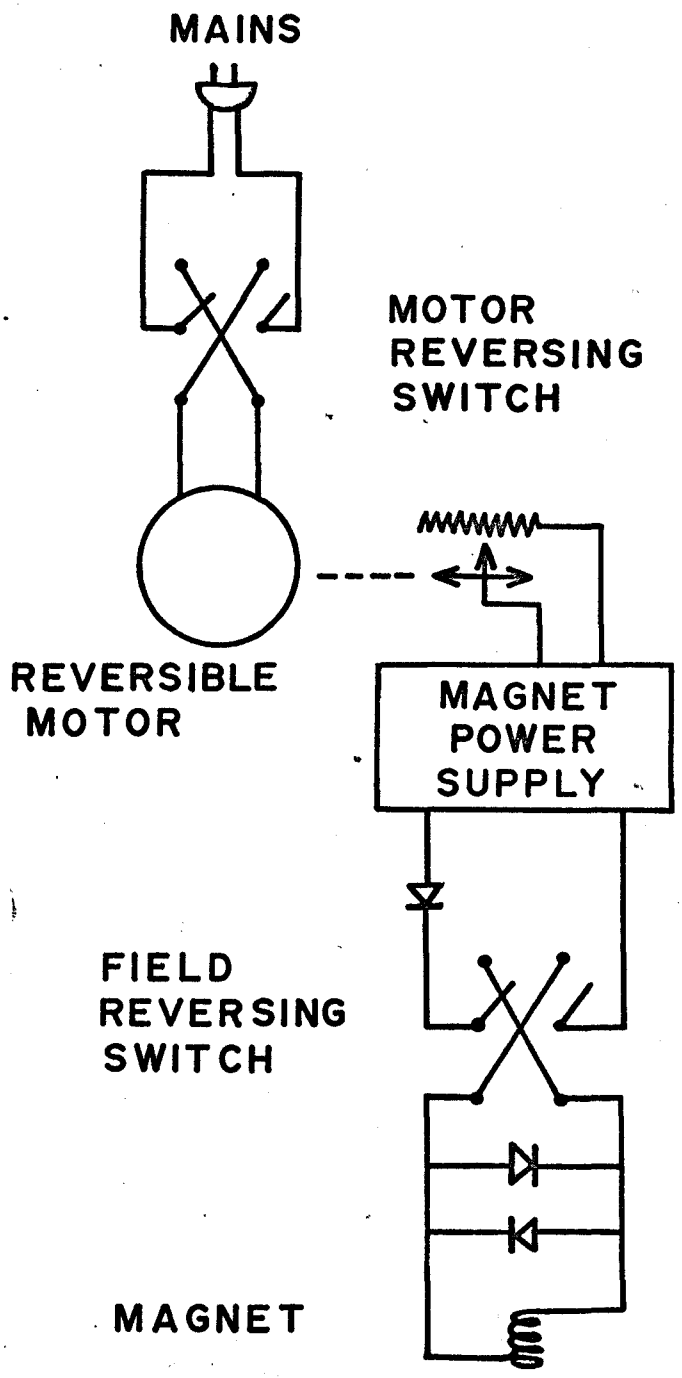
MAINS
MOTOR
REVERSING
SWITCH
REVERSIBLE
MOTOR
MAGNET
POWER
SUPPLY
FIELD
REVERSING
SWITCH
MAGNET

The source is placed in a 1/8 inch diameter stainless steel tube, which has been slit longitudinally, and which is mounted on an aluminum pedestal screwed to the bottom of the magnet. An aluminum pin fastened to the top of the magnet holds the sample firmly in position. Two coils of fine copper wire, of about 50 turns apiece, are wound around the tube; these form a miniature transformer, with the sample acting as part of the core. A sine wave signal is fed into this transformer, and the output signal is amplified and viewed on an oscilloscope. As the magnetic field is increased, and the sample becomes saturated, the amplitude of the output signal drops to a minimum and levels off.

Since the volume of the sample is much smaller than the volume of the transformer core, a second similar transformer has been mounted outside the cryostat, with its windings in series with those of the saturation testing transformer. In this second transformer, a small iron pellet mounted on the end of a brass screw makes it possible to tune out the constant portion of the output signal, which is due to the non-ferromagnetic part of the core, signal pick-up in the leads, etc.

The source holder and saturation transformer can be seen in the center of the magnet in Fig. III-4. A schematic of the saturation testing system is shown in Fig. III-5.

Fig. III-4. The magnet and detectors. The source holder-saturation testing transformer can be seen between the magnet coils. The detectors are in the positions they would occupy during an experiment.

Fig. III-5. A schematic of the saturation testing unit.

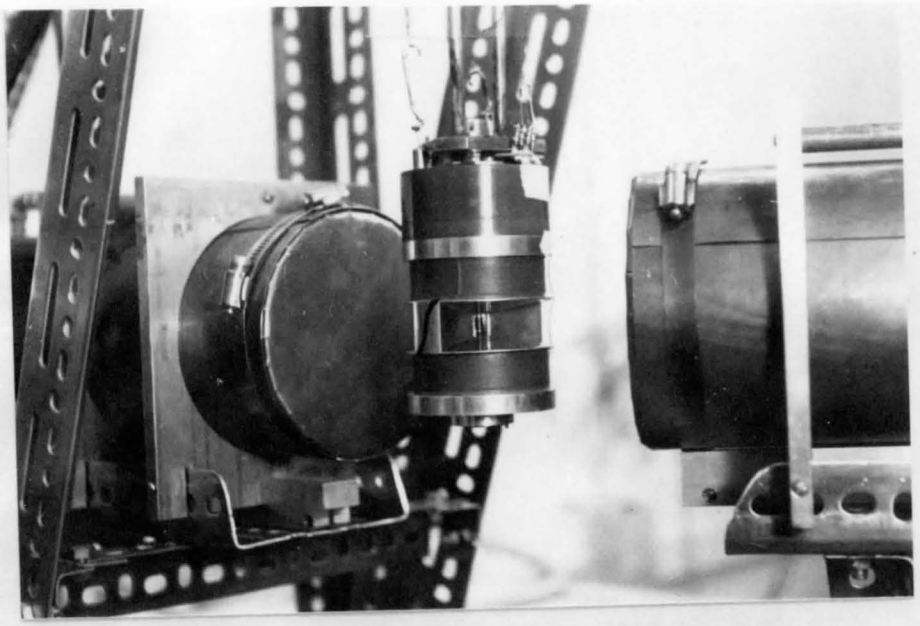

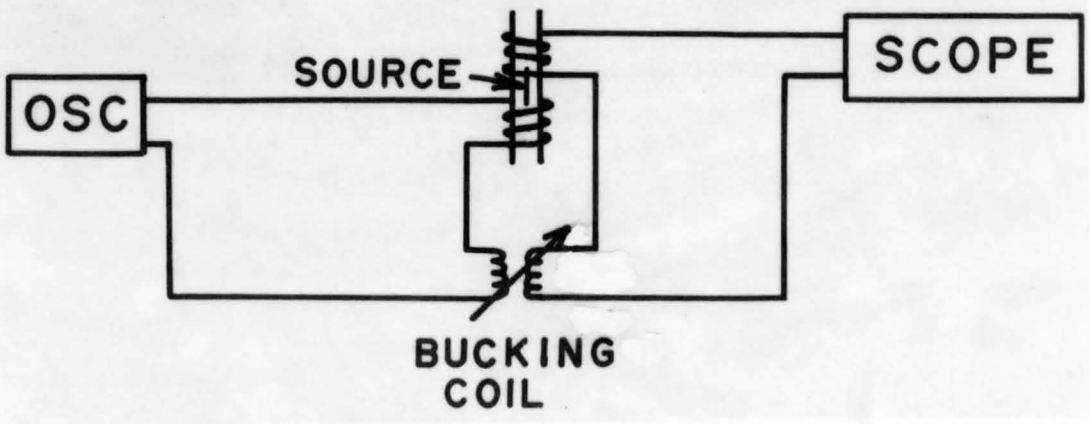
SOURCE
OSC
SCOPE
BUCKING
COIL

5. Magnetic Shielding

The output from photomultiplier tubes is very sensitive to the presence of a magnetic field. Thus, in order to place the detector crystals as close as possible to the source, it was necessary either to use long light pipes and set the photomultipliers well back from the source and field, or to provide some form of magnetic shielding for the tubes. The first alternative presents large potential problems in successfully optically coupling the crystal to the photomultiplier tube without a serious loss of resolution. The second alternative permits the use of integrally mounted detectors with their inherently greater resolution, provided that the fields can be reduced to a suitable level. The second alternative was chosen.

The magnetic shields are shown in Fig. III-4; fig. III-6 shows the details of construction. Sheets of Netic and Conetic AA, high permeability steel from Perfection Mica Co., were formed into three concentric cylinders separated by aluminum spacers, such that the successively larger diameter cylinders overlapped the inner ones slightly at both ends. A Netic cap was fitted over the end of the shield facing the field, with a thin aluminum disc to ensure that only the outer (Netic) cylinder is in contact with the cap.

Flux inside and outside the shield was measured with a sensitive gaussmeter for magnet currents up to 15

Fig. III-6. Details of the magnetic shield construction.

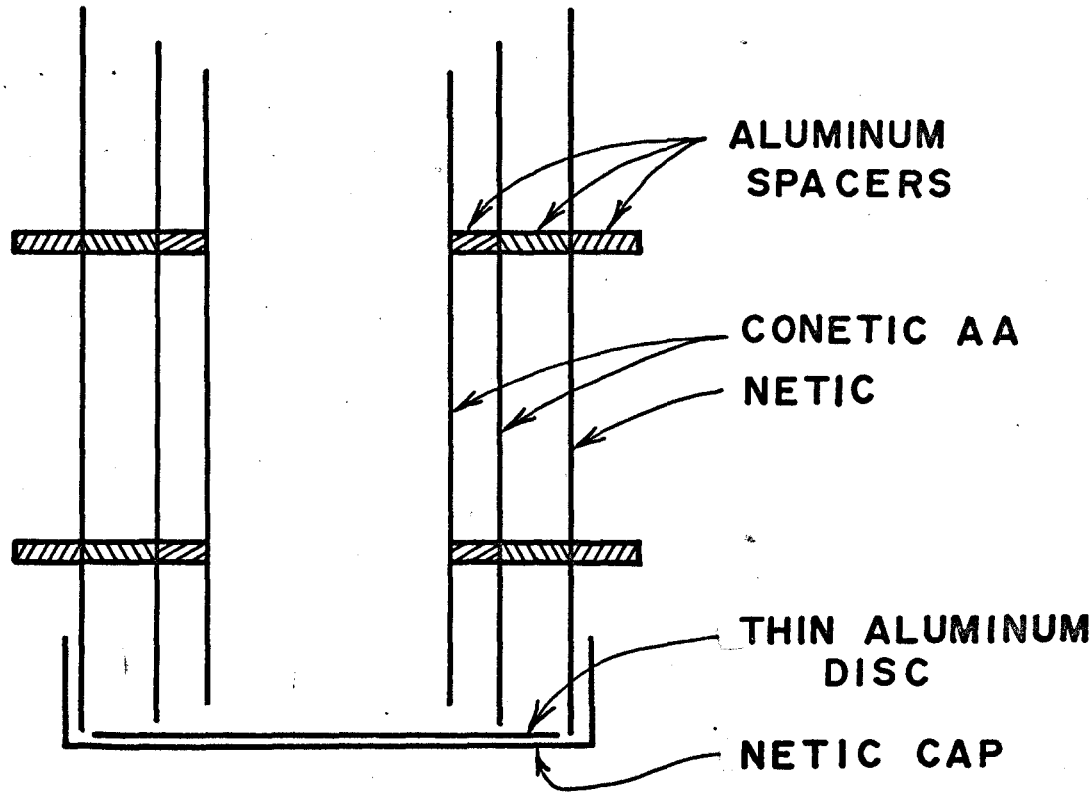
ALUMINUM
SPACERS
CONETIC AA
NETIC
THIN ALUMINUM
DISC
NETIC CAP

amperes. Maximum flux inside the shield at the approximate position of the photo-cathode was found to be about 90 milligauss; flux outside the shield at the corresponding distance from the magnet was about 100 gauss at 15 amperes. While the field outside the shielding decreased with distance from the center of the magnet as $\frac{1}{r^3}$, the flux inside the shielding was roughly constant from 4 cm from the end cap, outwards along the axis of the shield.

6. Data Collection System and Technique

The detectors used in this system are 2" x 2" NaI(Tl) crystals, optically coupled to RCA 6342A photomultiplier tubes. The NaI(Tl) scintillator provides high detection efficiency and a response function which is nearly linear with energy.

The fluorescent radiation produced by the interaction between the gamma ray and the crystal is detected in a photomultiplier tube; the signal is amplified, and a current pulse is emitted which is proportional to the energy of the incident gamma ray. This pulse passes directly into a charge-sensitive preamplifier, mounted directly behind the dynode chain to minimize noise pickup.

The preamplifier pulse is fed into a Sturrup 101 linear amplifier, and is reshaped to a flat-topped bipolar pulse whose height is proportional to the energy of the gamma ray. This pulse enters the Sturrup 501 fast-slow

discriminator single channel analyzer, which produces two output pulses; one is a very sharp timing pulse, derived from the cross-over point of the bipolar input pulse; the other is a logic pulse, which appears only if the height of the input pulse falls between the upper and lower discriminator levels.

A Sturrup 1401 fast-slow coincidence box determines whether the pulses from the two detectors are in coincidence. Single channel analysers on each of the detectors look at one of the gammas of the cascade being studied, and their fast and slow output pulses are fed into the coincidence box, which in turn emits a logic pulse if both the two fast pulses and the two slow pulses are in coincidence, and if the fast and slow coincidences are in coincidence with each other. The output pulse thus signifies that both gammas of the cascade have been seen within the resolving time of the circuit. A pulse delay line can be introduced into either of the single channel analyzers to determine the number of chance coincidences, events which occur when two gammas in the selected energy ranges but which have originated from different nuclei happen to arrive simultaneously.

To take full advantage of the detectors, two single-channel analyzers are used with each, to select both gammas of the cascade from each detector spectrum. If the gammas are denoted as A and B, and the fixed and moving detectors

as 1 and 2 then coincidences are recorded between the pairs (a) 1A - 2B and (b) 1B - 2A in separate coincidence boxes. However, for a given angle, the coincidence 1A-2B with the field "up" is completely equivalent to the coincidence 1B-2A with field "down"; thus for a given field direction, one pair produces a number of coincidences increased from the zero field case, and the other pair produces a decreased number. With the field in one direction, the number of coincidences (a) is recorded in scaler 1, and (b) in scaler 2; when the field is reversed (a) and (b) are recorded in the opposite scalers. In this way, scalers 1 and 2 simultaneously record $W(\theta,H)$ and $W(\theta,-H)$. The data collection system is shown schematically in figure III-7.

The coincidence outputs (a) and (b) are switched automatically by the pulse routing box, shown schematically in figure III-8. It is vital that data be taken for equal periods of time with the field "up" and "down". This is controlled by the clock scaler, which counts the pulses from the 60 cycle main power line and emits a signal pulse after a predetermined number has been reached. This pulse triggers the monostable and changes the state of the bistable in the routing box, which exchanges the scaler inputs.

Pulses from coincidence output (a) pass through gates 1 or 2 to scaler 1 or 2; similarly, pulses from (b)

Fig. III-7. The data collection system

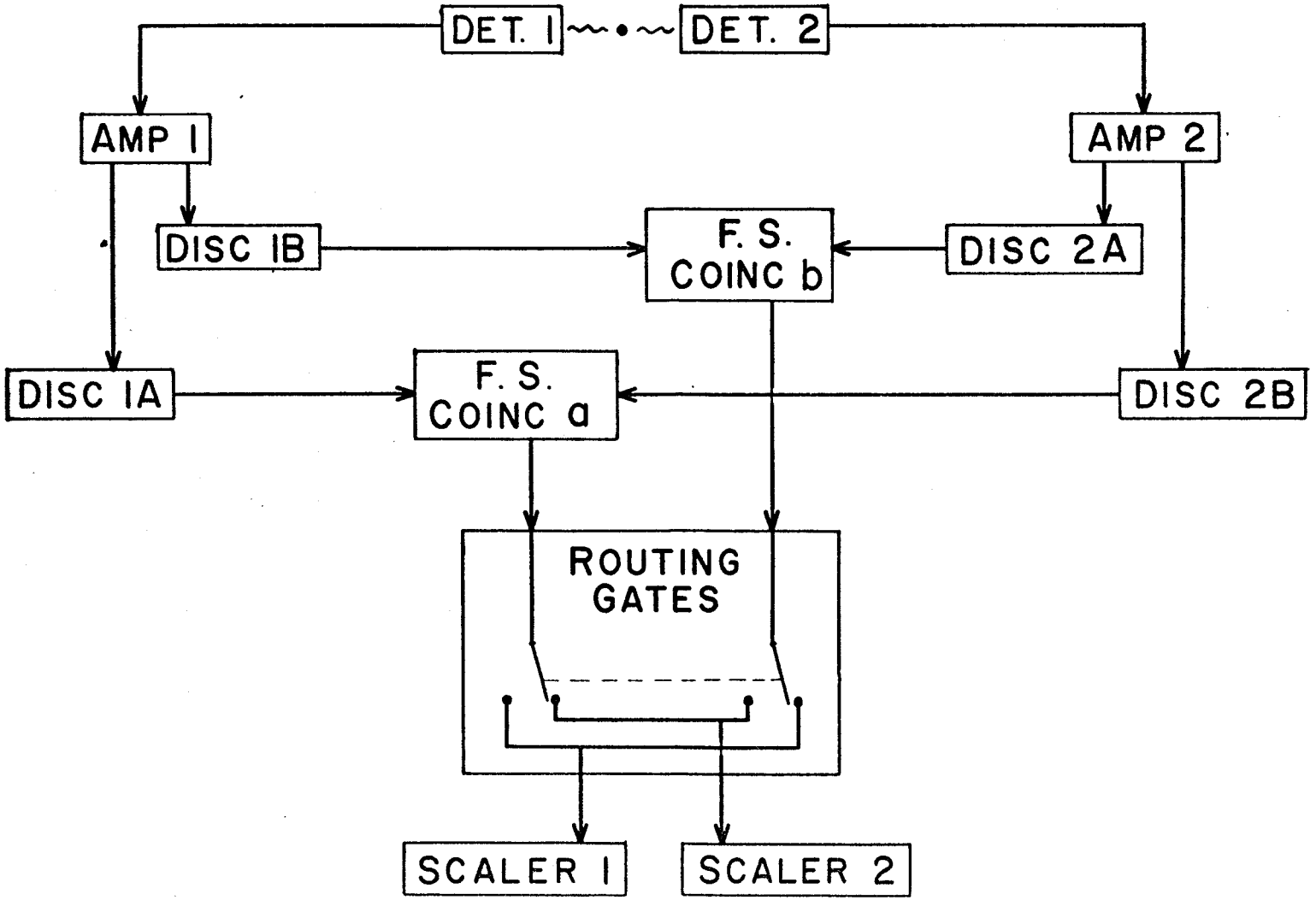
DET. 1
DET. 2
AMP 1
AMP 2
DISC 1B
F. S.
COINC b
DISC 2A
DISC 1A
F. S.
COINC a
DISC 2B
ROUTING
GATES
SCALER 1
SCALER 2

Fig. III-8. The pulse routing system.

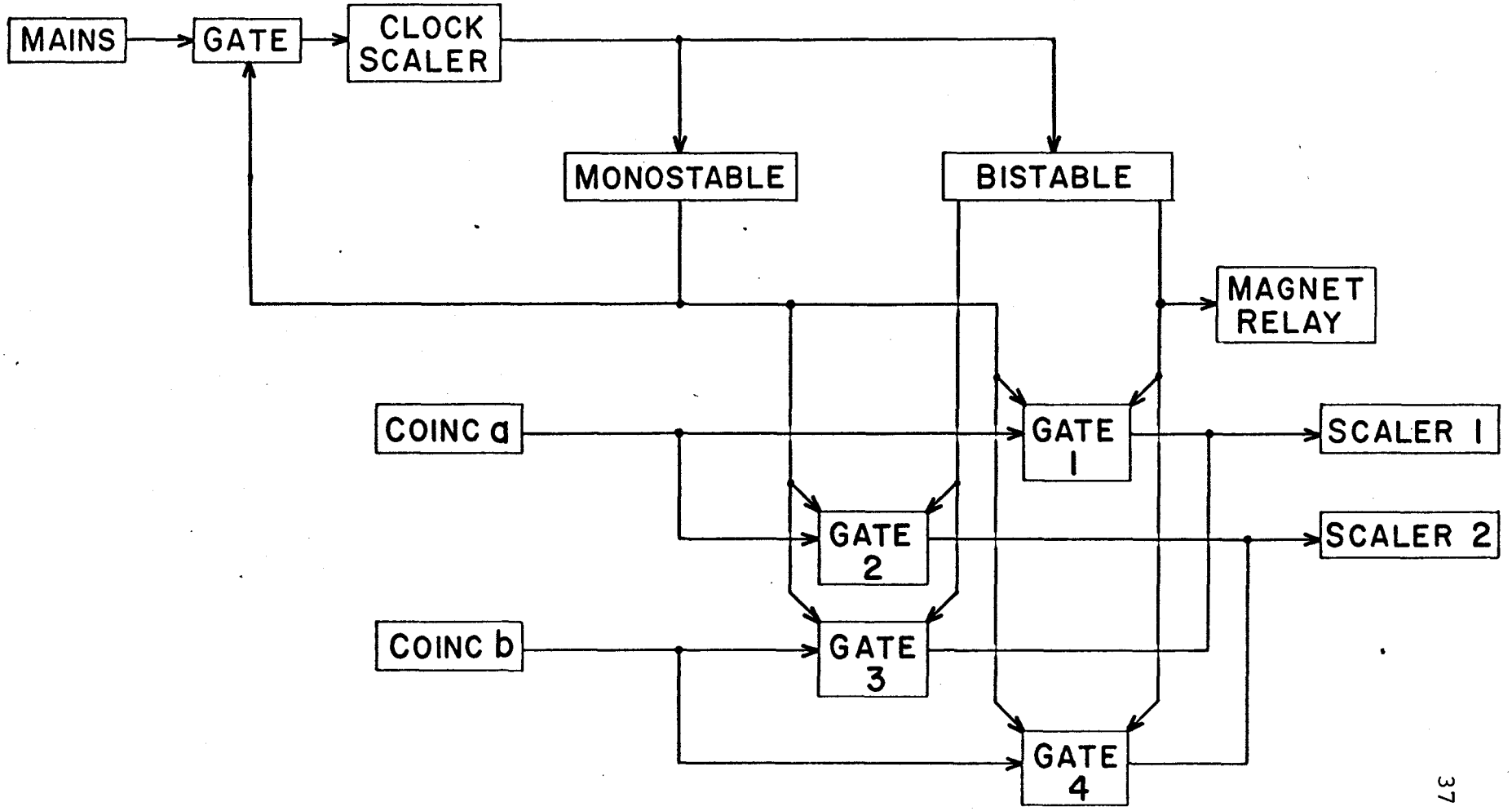
MAINS
GATE
CLOCK SCALER
MONOSTABLE
BISTABLE
MAGNET RELAY
COINC a
GATE 1
SCALER 1
GATE 2
SCALER 2
COINC b
GATE 3
GATE 4

pass through gate 3 or 4 to scaler 1 or 2. The bistable open circuits either gates 2 and 3 or 1 and 4; thus coincidence outputs (a) and (b) feed scalers 1 and 2 or 2 and 1 respectively, depending on the state of the bistable.

In the original apparatus, the bistable also controlled the state of a relay reversing switch, which changes the field direction by reversing the current flowing through the magnet. The purpose of the monostable is to temporarily open circuit all the gates, and also the gate passing the 60 cycle pulses to the clock scaler, until transients arising from the sudden reversal of current in the magnet have died out. The current flowing in a superconducting magnet can not be abruptly reversed, however; it must be slowly reduced to zero, then reversed, and slowly increased to the desired value again. Not shown in figure III-8 is a switch which, when closed, will hold the monostable in the open state indefinitely on receipt of the next pulse. When the low temperature system is in use, this switch is closed immediately each time counting is begun. The counting is then stopped as soon as the clock scaler emits a pulse. The magnet current is then slowly reversed, according to the procedure discussed in par. III-3. Once the desired magnet current has been reached, the monostable is released, and the cycle begins again.

A readout meter is used to correlate visually the bistable state with the field direction.

7. Stabilizing System

A negative feedback system is used to stabilize the gain of the photomultiplier tube and amplifier against short term drift. The amplifier output is fed into a third single channel analyzer,which is set to look at some prominent peak in the spectrum. A small amplitude signal from a low frequency (about 20 Hz) oscillator is added to the base line voltage of the window, after passing through a phase shifter, thus swinging the window periodically across the peak, and modulating the number of pulses put out by the analyser. These pulses pass through a pulse stretcher, to form a very noisy but continuous signal. The oscillator frequency component is extracted by a twin tee tuned amplifier, and compared with the original oscillator signal by means of a phase-sensitive detector. The output from the phase-sensitive detector controls the grid bias of a triode tube which is placed in series with the dynode chain of the photomultiplier tube. This varies the voltage drop across the tube, and thus varies the voltage (and gain) of the photomultiplier tube. This system is shown schematically in Figure III-9.

If the gain of the photomultiplier and amplifier is such that the peak is centered in the window, the window

Fig. III-9. A schematic of the "window wobbler" stabilizing system.

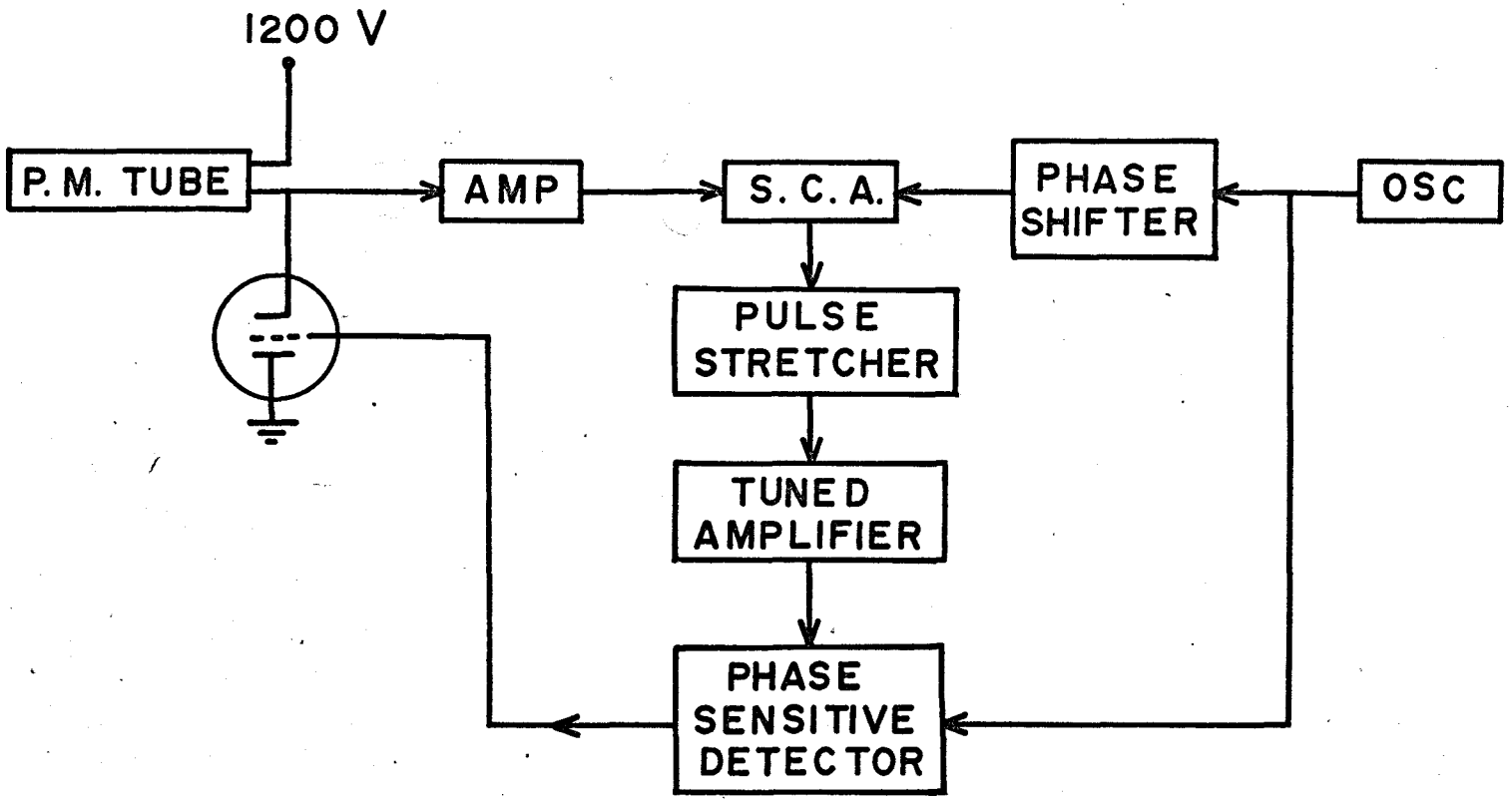
1200 V
P. M. TUBE
AMP
S. C. A.
PHASE SHIFTER
OSC
PULSE STRETCHER
TUNED AMPLIFIER
PHASE SENSITIVE DETECTOR

is swung symmetrically across the peak and the number of pulses reaches a maximum twice during the cycle, as the window passes over the peak when rising or falling. The output is thus modulated at twice the oscillator frequency, and the tuned amplifier output has very small amplitude. If the gain shifts slightly, an oscillator frequency component begins to appear; the phase of this component depends whether the gain has increased or decreased, and its amplitude depends on the magnitude of the shift. The phase and amplitude of the tuned amplifier output relative to the oscillator determines the polarity and magnitude of the phase sensitive detector output,and hence determines the correction to the voltage across the dynode chain.

To minimize the effects of long term drift, field direction is reversed frequently. This method becomes more and more effective as the frequency of field reversal increases, but as it takes several minutes to reverse the field a compromise must be reached with the loss of counting time during field reversal.

As a precaution against systematic effects in the apparatus, eight configurations are used in sequence. After every second set of readings, the angle of the moving

counter with respect to the fixed counter is changed to its equivalent position about 180^{o}; after every other set, the window in each of the single channel analyzers is changed to look at the other gamma in the cascade. After every four sets, the direction of the field with respect to the bistable state is reversed. Four counting cycles are used in each set.

CHAPTER IV

EXPERIMENTAL

The first experiment to be performed on the low temperature apparatus was a measurement of the rotation of the 966.4 keV gamma-vibrational state of ^{160}Dy, by observing the shift of the angular correlation of the 298.5 - 966.4 keV cascade following the β^- decay of ^{160}Tb. This experiment was performed at liquid helium temperature with the decaying nuclei in terbium metal.

1. Spectrum and Decay

The gamma spectrum of ^{160}Tb is extremely complex; more than 100 gamma rays have been identified. A simplified decay scheme is shown in Fig. IV-1. While most of these radiations have very low intensity, the result is a very high background. This is clearly shown in the NaI spectrum in Fig. IV-2. This presents problems for two reasons. First, there is an upper limit to the total number of counts the detector can accept (empirically about two million per minute) before the resolution begins to deteriorate. Hence the strength of the sources is limited, and as a result the fraction of the desired gammas to the total number is effectively reduced. Secondly, it makes the

Fig. IV-1. A simplified decay scheme of ^{160}Tb. The intensities of the important radiations are

216 keV	3.8%
298.5	26 %
310	0.9%
337	0.39%
392	1.6%
879.4	31 %
962.6	8.8%
966.4	25 %

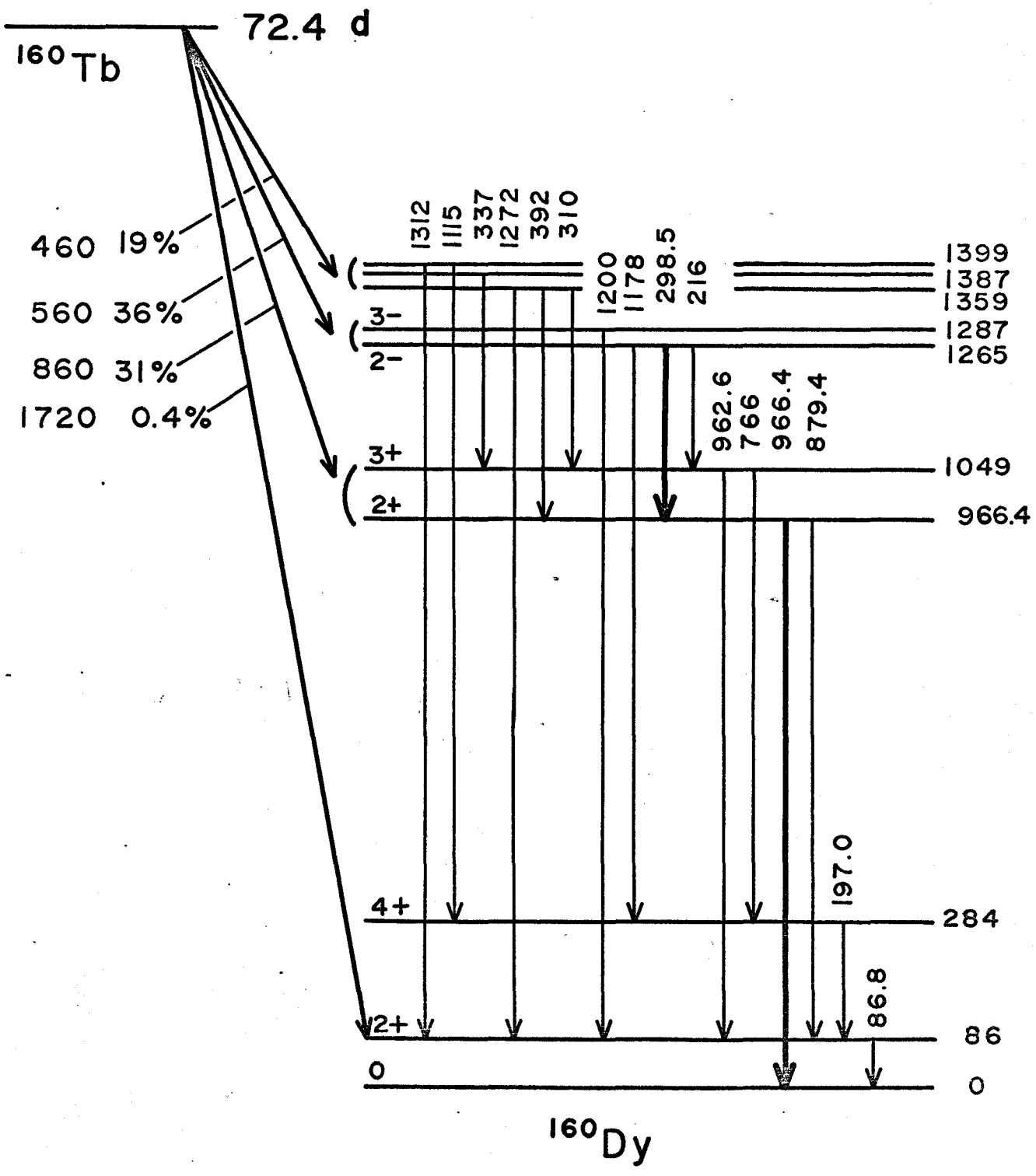
72.4 d
160Tb
460 19%
560 36%
860 31%
1720 0.4%
1312
1115
337
1272
392
310
1200
1178
298.5
216
962.6
766
966.4
879.4
197.0
86.8
1399
1387
1359
1287
1265
1049
966.4
284
86
0
3-
2-
3+
2+
4+
2+
0
160Dy

Fig. IV-2. The NaI spectrum of the ^{160}Tb decay. The curves marked 400A and 400B are the spectra seen in coincidence with the windows A and B, with counts per channel multiplied by 400. These spectra were taken during an experimental run.

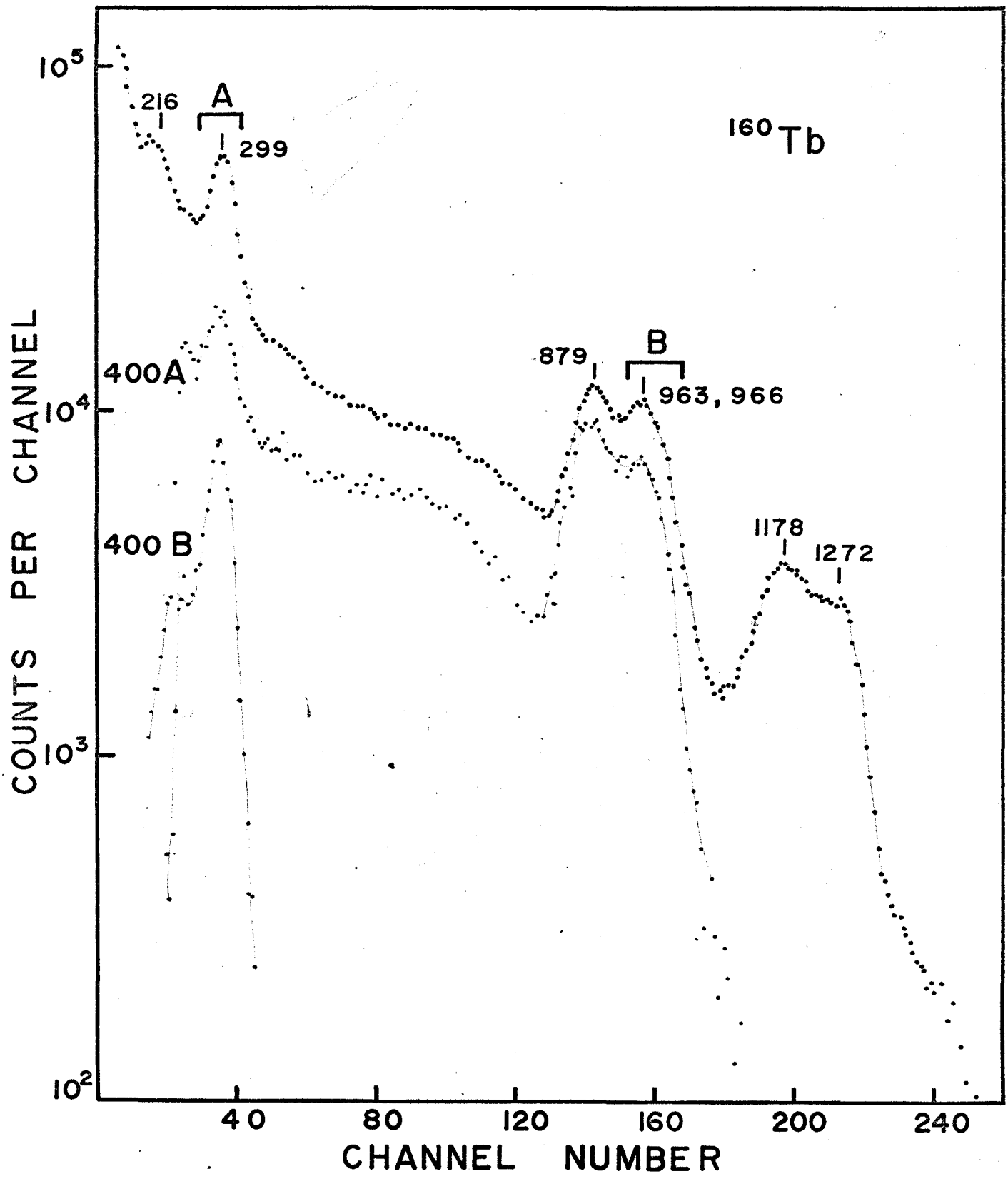
10^5
10^4
10^3
10^2
COUNTS PER CHANNEL
216
A
299
^{160}Tb
400A
879
B
963, 966
400 B
1178
1272
40
80
120
160
200
240
CHANNEL NUMBER

Fig. IV-3. A partial spectrum obtained from a high resolution solid state detector. The intensities of the lines have not been corrected for detector efficiency.

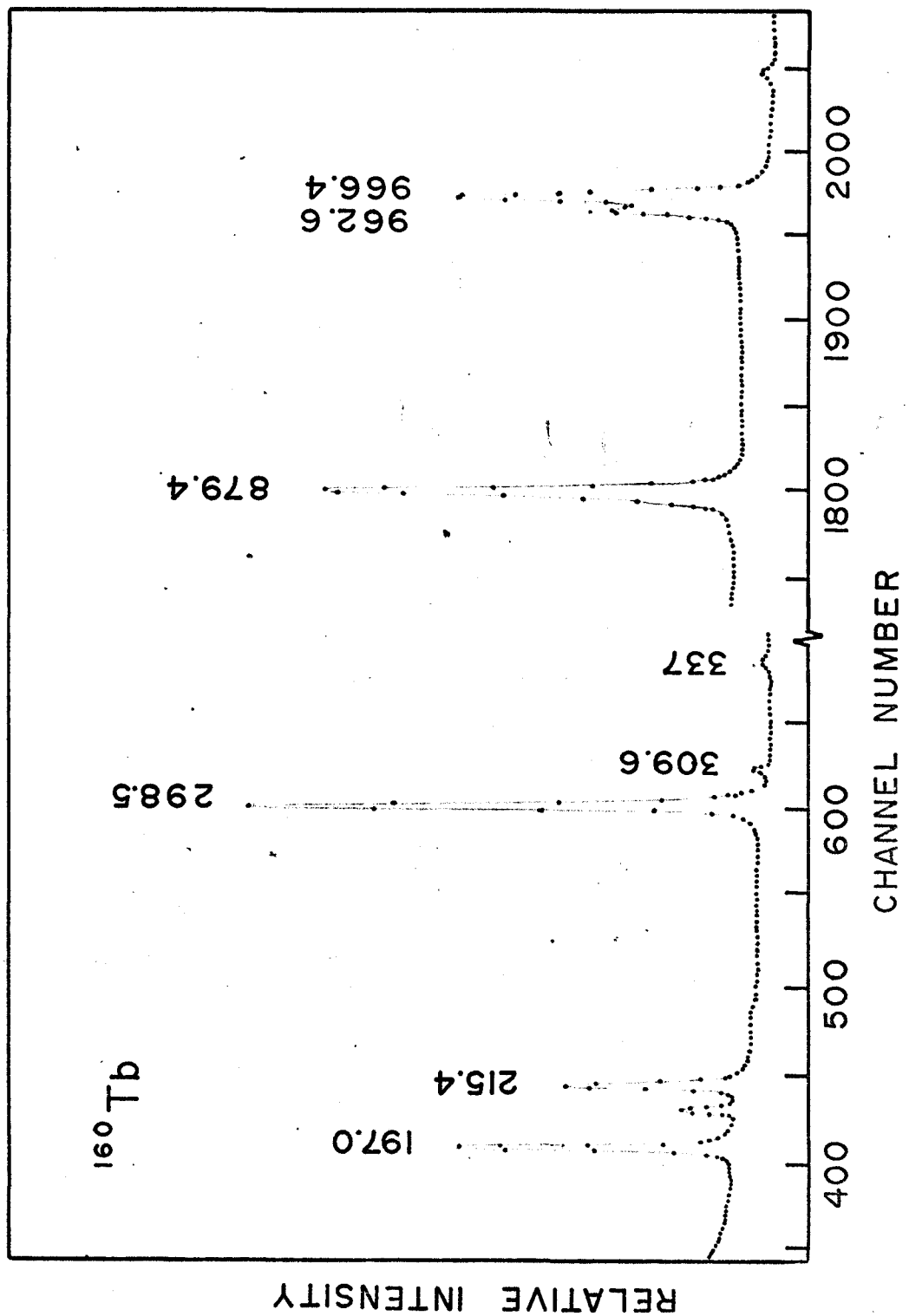
RELATIVE INTENSITY
CHANNEL NUMBER
400
500
600
1800
1900
2000
^{160}Tb
197.0
215.4
298.5
309.6
337
879.4
962.6
966.4

tuning of the feedback circuit more difficult. The feedback circuit window was locked onto the 879.4-966.4 double peak, which has a peak-to-valley ratio of two to one on the low energy side; this severely limits the amplitude of oscillation of the window, and results in a low signal-to-noise ratio on the feedback signal. The signal-to-noise ratio is further reduced by the necessity of straddling the double peak. Stability of the upper peak is much more critical than stability of the lower peak. The 879.4 keV peak is also in coincidence with the 298.5, and the 298.5-879.4 angular correlation is comparable in magnitude with the 298.5-966.4 but of opposite sign. For this reason, the window on the 966.4 keV peak is set high. Since the same windows were used to measure the unperturbed angular correlation, the contribution from the 298.5-879.4 cascade is automatically corrected for.

Fig. IV-2 also shows the coincidence spectra, obtained by taking the spectrum from one amplifier in coincidence with pulses from the single channel anayzers set to windows A and B on the other side. These spectra were obtained from a Nuclear Data Series One-Twenty 512 channel analyzer, and were taken during an actual run in the liquid helium apparatus.

The partial spectrum in Fig. IV-3, obtained using a lithium-drifted germanium detector, shows the finer details

in the regions of the two peaks of interest.

The 298.5-966.4 cascade is particularly favourable from the point of view of corrections for competing cascades. The two gammas have high relative intensities, appearing in 26% and 25% of the ^{160}Tb decays respectively; the coincidence rate is correspondingly high. The higher energy photon is second in the cascade and goes to the ground state. There are no gammas leading into the initial (1265 keV) state with energies high enough to produce Compton events lying in the window of the second radiation; this would result in a "true" coincidence being counted for a cascade through a different state. While Comptons from the 392 keV radiation will produce true coincidences, the 392-966.4 cascade passes through the level being studied, and measurement of the unperturbed angular correlation would take this into account. As mentioned previously, the small contributions from the 298.5-879.4 cascade would also be automatically corrected for.

The gammas passing through the 1049 keV state pose a more serious potential problem. This level decays predominantly through emission of a 962.6 keV gamma, with a relative intensity of 8.8%, which will certainly be seen in the higher energy window. The rotation of this state should be about the same as the 966.4 keV state; their g-values should be the same, since they are members of the same

rotational band, and their lifetimes should be quite similar. However, contributions from cascades through this level can be neglected for the following reasons. The 216 keV gamma should not be seen at all in the low energy window. The 309.6 keV line will appear to a large extent in the low window, but its intensity is quite low at 0.9%, and also the anisotropy of a 2^{-}-3^{+}-2^{+} cascade is very small. The spin of the initial state of the 337 keV gamma is not known, so the anisotropy of the 337-962.6 cascade can not be calculated; however, the intensity of this radiation is only 0.39%, and also the window for the 298.5 keV peak should fall in the valley between the 337 keV photopeak and its Compton edge.

2. Sources

Sources were activated by neutron capture in terbium metal in the McMaster reactor. As terbium metal consists entirely of the isotope ^{159}Tb, and as ^{160}Tb decays only from its ground state by β- decay to ^{160}Dy, there were no problems created by the presence of other decay modes. A high resolution spectrum plot showed that there were no radioactive contaminants.

The terbium was obtained from K & K Laboratories Inc. (New York), in the form of metal shavings. The metal appeared to deteriorate slightly with time, becoming more brittle. The first source was made from a single piece of

terbium, which was flattened into a rectangle about 2½ mm x 1 mm x 0.1 mm thick. The other source used consisted of three pieces, each slightly longer than it was wide. These were held together with a bit of masking tape, placed one above the other, aligned along their long dimensions. This arrangement results in a poorer demagnetizing factor however.

3. Measurement of the Unperturbed Angular Correlation

Because of the contributions from cascades other than the 298.5-966.4 cascade through the 966.4 keV level, the unperturbed angular correlation was measured using windows identical to those used in the magnetic measurements. This not only makes corrections to results obtained theoretically or in other laboratories unnecessary, it also automatically corrects for possible systematic effects in the apparatus.

Since the coil spacers on the superconducting magnet severely attenuate the gamma spectrum at 90^{o} and 270^{o}, it was necessary to perform the angular correlation measurement on another table. To duplicate the geometry of the low temperature apparatus as closely as possible, four glass cylinders of the same diameter and thickness as the wall of the dewars were placed concentrically about the source. The system used is shown in Fig. IV-5.

The source itself was mounted on a pedestal, and its position was adjusted until it was centered to within

1%. This was done by monitoring the singles rates of the 298.5 keV peak at 90^{o}, 180^{o}, and 270^{o}. The detectors were set at the same distance from the source as they would be during a low temperature run (8½ cm. for the first measurements, 10 cm. for the later ones).

Coincidence rates were measured every $22\frac{1}{2}^{o}$ from 90^{o} to 270^{o}. The clock scaler was used to ensure equal time durations for these runs. Chance coincidence measurements were taken at 90^{o}, 180^{o}, and 270^{o}. The corrected coincidence rates for pairs of angles symmetric about 180^{o} were added together, and the five values obtained were analyzed in a three-parameter least squares fit to give the coefficients b_n of the expansion

$$W(\theta) = b_o + b_2 \cos 2\theta + b_4 \cos 4\theta \ .$$

Normalizing to $B_o = 1$, the results obtained were

$$W(\theta) = 1 + (0.0875 \pm 0.0011) \cos 2\theta + (0.017 \pm 0.006) \cos 4\theta \quad \text{at } 8\tfrac{1}{2} \text{ cm.}$$

$$W(\theta) = 1 + (0.0869 \pm 0.0019) \cos 2\theta + (0.032 \pm 0.009) \cos 4\theta \quad \text{at 10 cm}$$

Solid angle correction factors tabulated by Yates (1964) show that B_2 should increase by about 1% and B_4 by about 4% as the detectors are moved from 8½ to 10 cm. Note that a small shift in one of the data points can change the relative values of B_2 and B_4 with only a slight altera-

tion in the maximum slope of $W(\theta)$, which is the point of interest. Since the corrections fall within the stated errors, the coefficients have been averaged, weighting the values to the number of counts obtained at each distance. This gives

$$W(\theta) = 1 + (0.0873 \pm 0.0008) \cos 2\theta + (0.022 \pm 0.004) \cos 4\theta \quad .$$

The numbers obtained represent averages over several measurements. The unperturbed angular correlation was measured at 8½ cm. just prior to, immediately after, and some time after the first magnetic run, and at 10 cm.immediately after the second magnetic run.

As a check on the reproducibility of the measurement, histograms of the values of the coefficients B_2 and B_4 obtained in the individual runs have been plotted in Fig. IV-4. The B_2 plot shows a definite peak at about 0.103, but with a much greater spread of points at lower values than are above the peak.

There are two possible explanations for this, both of which are related to the stability of the system. Since the windows on the 966.4 keV peak are set high on the peak, (ref. Fig. IV-2), a small shift in gain during the run could alter the coincidence rate. However, this effect alone would be as likely to increase as to decrease the value of B_2. A more likely explanation arises from the

Fig. IV-4. Histograms of the distributions of the anisotropy coefficients B_2 and B_4 obtained from the individual unperturbed angular correlation runs. The error bars show the statistical counting errors on the individual runs. The values were weighted to the b_o value for each run. The points • were obtained with the detectors at 8½ cm., and o at 10 cm. The points ♂ were deleted for the second calculation of B_2 and B_4.

$B_2 = 0.1003 \pm 0.0026$

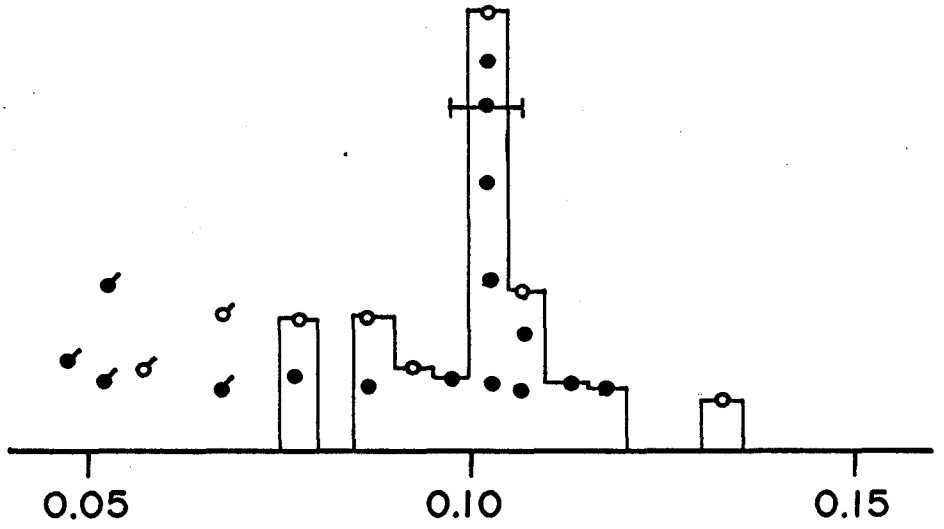

$B_4 = 0.0203 \pm 0.0025$

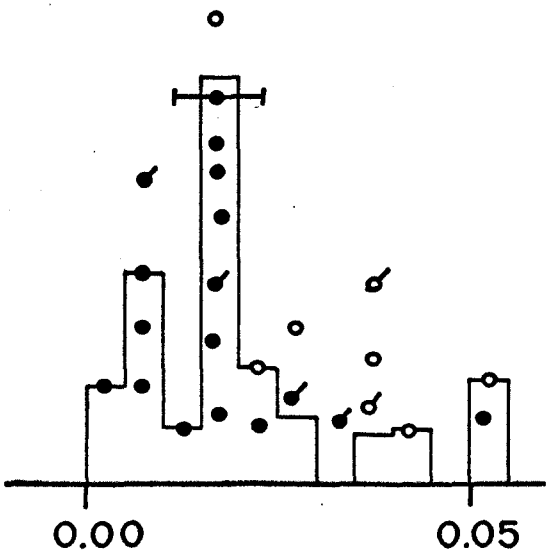

Fig. IV-5. The system used to measure the unperturbed angular correlation.

Fig. IV-6. The angular correlation pattern obtained.

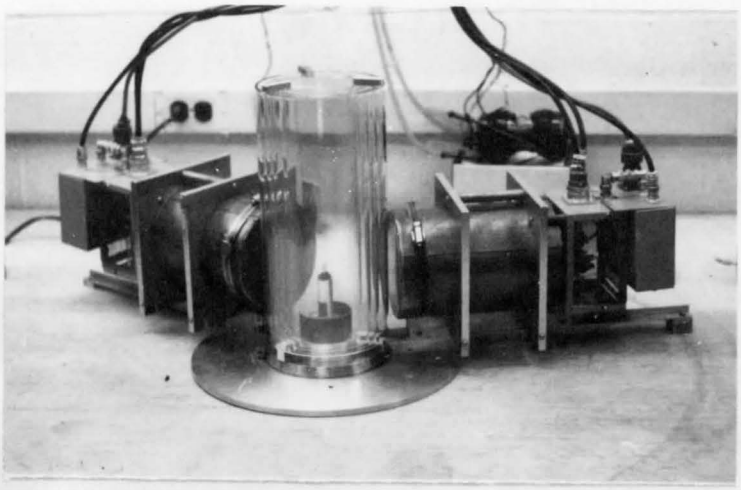

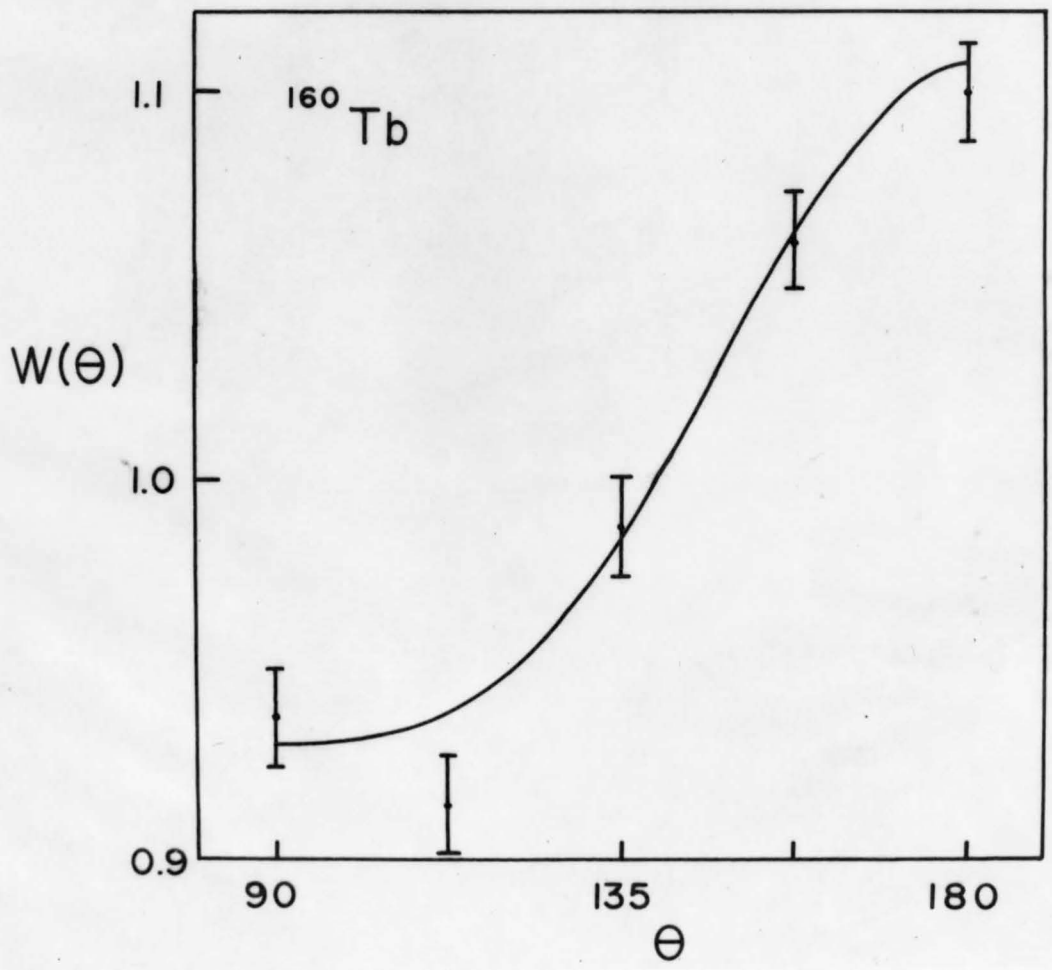
1.1
1.0
0.9
W(θ)
160 Tb
90
135
180
θ

298.5-879.4 cascade, which has a B_2 about half the size of the B_2 of the 298.5-966.4 cascade and of opposite sign. If this gain shifted in such a way as to increase the contribution from this cascade, the measured anisotropy could be significantly reduced.

In view of these considerations, the six measurements which gave the lowest values of B_2 were eliminated, and the anisotropy coefficients were recalculated. This gives values of B_2 and B_4 which agree quite well with the values obtained from the adjusted histogram:

	calculated	histogram
B_2	0.1012 ± 0.0011	0.1003 ± 0.0026
B_4	0.0205 ± 0.0059	0.0203 ± 0.0025

Taking the calculated values with the larger of the errors in each case gives the results

$$W(\theta) = 1 + (0.1012 \pm 0.0026)\cos 2\theta + (0.0205 \pm 0.0059)\cos 4\theta \quad .$$

This curve has been plotted in Fig. IV-6.

Quadrupole attenuation effects were calculated to be negligible.

4. Measurement of the Rotation

The perturbed angular correlation measurements were made essentially in two runs.

At the time of the first run, the magnetization saturation testing unit was functioning only marginally;

the tuning coil had not been added to the circuit, and the signal-to-noise ratio was quite low. The amplitude shift observed indicated that the sample (source number one) was saturating at a magnet current of five amperes, corresponding to a field of about 4.5 kilogauss. According to Thoburn, Legvold and Spedding (1958), the sample should be nearly saturated at this field; the magnetization curve keeps rising slowly past this point at a decreasing rate.

During the first run, the magnet current was 6 amperes, producing a field of 5.3 kilogauss. The detectors were mounted 8½ cm. from the source. Coincidence rates were measured at 150° and 210°. As mentioned previously, the field direction was reversed every 45 minutes, and either the detector angle or the single channel analyzer windows were changed after every four readings.

During the second run, the saturation tester was working well; typical results obtained during a saturation test are shown in Fig. IV-7. For this run the current was kept to 15 amperes (13.2 kilogauss). Coincidence rates were measured at 140° and 220°. Initially the detectors were mounted 8½ cm. from the source; they were later moved back to 10 cm. to reduce possible movement of the magnet due to forces exerted between the field gradient and the magnetic shielding around the detectors.

The single event count rates seen through each of

Fig. IV-7. A curve showing the magnetic saturation of the source used in the second run. The points on this curve show the average of the amplitudes obtained over six runs.

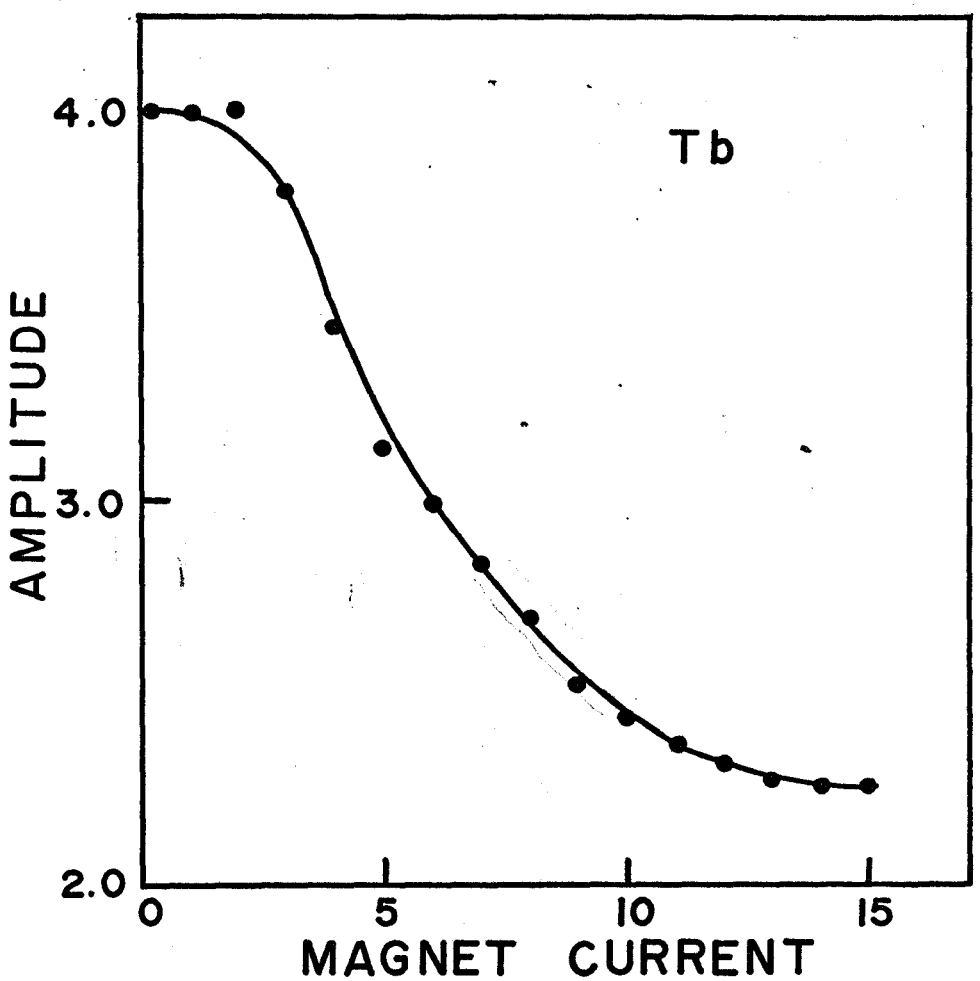
Tb
AMPLITUDE
4.0
3.0
2.0
0
5
10
15
MAGNET CURRENT

the single channel analyser windows were measured throughout the experiment, and it became apparent as the experiment progressed that these were beginning to fluctuate. Several sets of readings were eliminated from the second run because of this; the criterion used was a maximum acceptable variation in count rate of 2% for the 966.4 keV peak and 3% for the 298.5 keV peak. No variations of this size were observed in the first run. Because of the periodic switching of the field direction, the magnetic runs should be less sensitive than the angular correlation measurements to long term drifts in the electronics.

The values of $\frac{R}{2}$ obtained from the individual sets of readings were plotted in histogram form, as shown in Fig. IV-8, to check their deviation from the mean. Although the small number of points makes the histograms rather crude, the standard errors obtained from them agree very well with the errors expected from the numbers of counts obtained in the runs. The mean values of $\frac{R}{2}$ obtained were:

	calculated from data	from histogram
first run (8½ cm.)	0.00358 ± 0.00073	0.0037 ± 0.00075
second run (8½ cm.)	0.00497 ± 0.00182	0.0050 ± 0.0021
(10 cm.)	0.00381 ± 0.00183	0.0039 ± 0.00017

Using the calculated values with the final expression for $W(\theta)$ gives the following values for $\omega\tau$:

Fig. IV-8. Histograms of the distributions of the values of the measured parameter $\frac{R}{2}$ (times 1000). The error bars show the statistical error for each measurement. The points o were obtained at 8½ cm, ● at 10 cm.

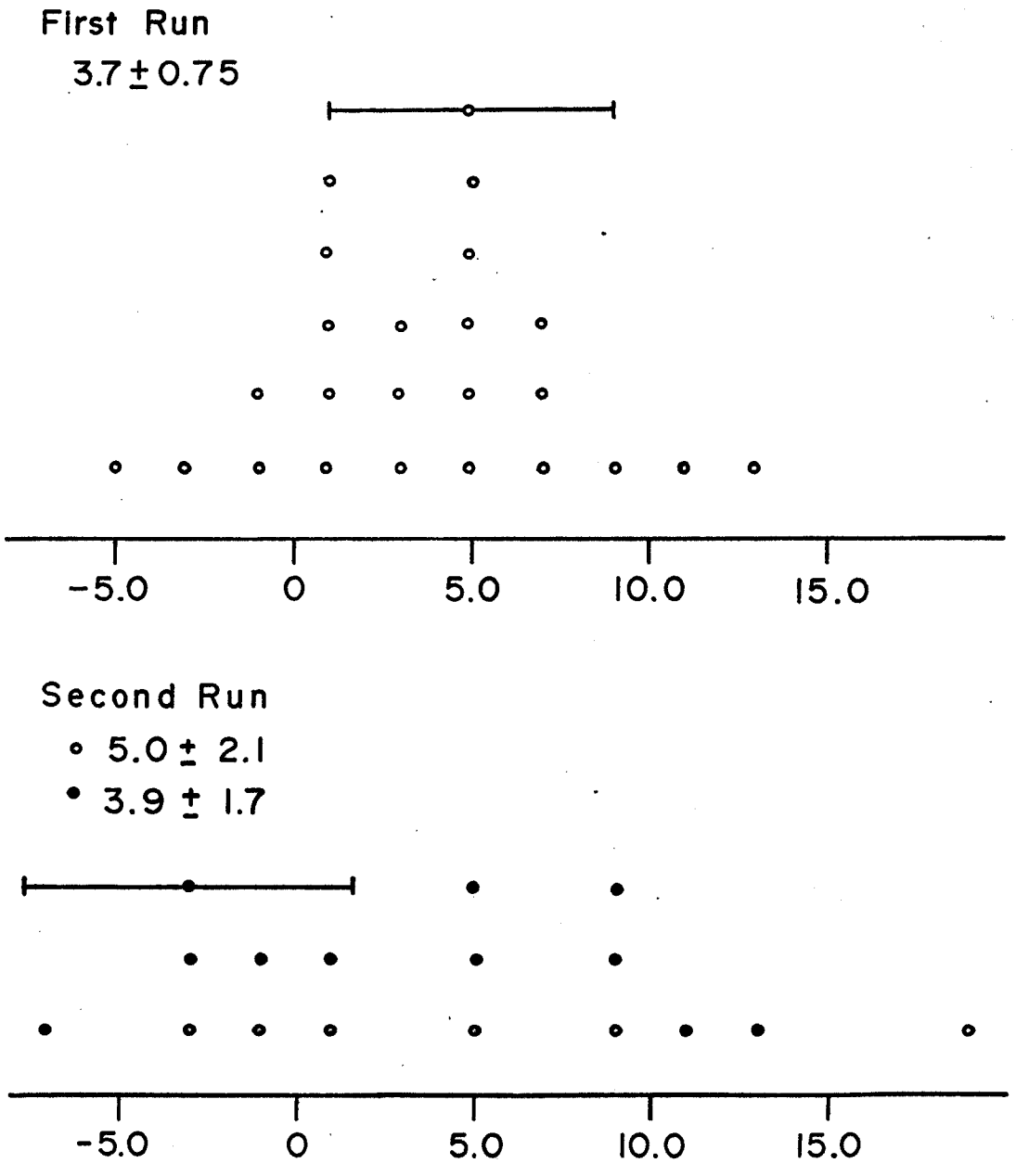
First Run
3.7 ± 0.75
-5.0
0
5.0
10.0
15.0
Second Run
○ 5.0 ± 2.1
● 3.9 ± 1.7
-5.0
0
5.0
10.0
15.0

first run	-0.0150 ± 0.0040
second run	-0.0218 ± 0.0080
	-0.0167 ± 0.0087

These values of $\omega\tau$ were averaged, weighted by the total number of coincidences obtained during each run, to give the result

$$\omega\tau = -0.0161 \pm 0.0033.$$

Since terbium is ferromagnetic only in the c planes, the atomic moments are only partially aligned with the magnetic field, and hence the measured value is only an effective rotation. To a first approximation, the observed rotation is found to be $\frac{\pi}{4}$ of the actual rotation. Correcting the measured value gives the result

$$\omega\tau = -0.0215 \pm 0.0044 \text{ radians.}$$

A dummy run was also performed following the second run, to check for systematic effects in the apparatus. The experiment was repeated at zero field; the results of this run were

$$\frac{R}{2} = 0.0001 \pm 0.0014..$$

5. Discussion

Neither the lifetime τ of the 966.4 keV state nor the internal field at a dysprosium nucleus in a terbium lattice has been measured directly.

The state lifetime can be obtained from the B(E2) value, measured by Coulomb excitation to be $(0.069 \pm 0.020)\ e^2.10^{-48}\ cm^4$ for the 966.4 k3V level (Yoshizawa et al., 1965). Since the B(E2) is proportional to the $\langle J_i \lambda K_i K_f - K_i | J_f K_f \rangle^2$, the B(E2) for decay to the ground state is given by

$$\frac{\langle 2222 | 00 \rangle^2}{\langle 0202 | 22 \rangle^2} \; B(E2)_{ex} = \frac{1}{5} B(E2)_{ex}.$$

The transition probability is given by

$$T(E2)_{966.4} = \frac{4\pi}{75} \frac{k^5}{\hbar} \frac{B(E2)_{966.4\ ex}}{5}.$$

Then, correcting for the intensities of the other transitions from the 966.4 keV level, the lifetime of the state is given by

$$\tau = \frac{1}{T(E2)_{total}} = (3.1 \pm 0.9) \times 10^{-12} \text{ sec.}$$

Using this value and the measured value of

$$\omega\tau = \frac{g\mu_N H}{\hbar} \tau$$

the product $gH = (-1.4 \pm .7) \times 10^6$ gauss can be obtained .

Since the most significant factor in the effective field at the nucleus for the rare earths is the 4f orbital angular momentum term (ref. Chapter II), one might expect the internal field at the nucleus of an atom placed in the lattice of another element to depend less on the host than on the impurity itself. The value of the effective field at the nucleus in dysprosium metal has been measured by Kobayashi, Sano and Itoh (1966). Using their value of the magnetic interaction frequency for ^{161}Dy, 830 Mc/sec, and the value $\mu = 0.42$ from Nuclear Data Sheets, Appendix 1, $H_{eff} = 6500$ k0e. Using this value, we obtain

$$g = .23 \pm .11$$

for the g-value of the 966.4 keV state in ^{160}Dy. This value must be regarded as speculative because of the assumptions involved.

The rotation of the 966.4 keV state has also been observed by Kundig (1961); this experiment was done in liquid air. He measured the parameter $R = (5.9 \pm 1.6) \times 10^{-3}$; using his stated values of the angular correlation coefficients, this gives a rotation $\omega\tau = 9.9 \pm 2.7$ milliradians, which is in reasonable agreement with the present measurement. No correction was made for the distribution of moments.

CHAPTER V

CONCLUSION

It has been demonstrated that perturbed angular correlation experiments can be performed in the ferromagnetic rare earth elements, in spite of problems arising from complex decay schemes and high stability requirements on the electronics. Significant improvements could be made to the apparatus in this respect; higher stability power supplies and stabilizing systems employing much higher feedback gain would be good first steps.

There are several other ways in which the apparatus can be improved. A device to permit the mounting of sources without completely disassembling the dewars would be convenient. A more efficient method of testing saturation would be useful. Perhaps a bridge circuit sensitive to small changes in inductance could be used, or perhaps the sample could be passed rapidly through the coil and the inductive voltage pulse measured on a ballistic galvonometer. A significant improvement from the point of view of operator tedium would be an automated field reversing circuit.

It might be worth while to adopt another approach

to the collection of data, and record the whole coincidence spectrum on a multi channel analyzer. The data could be analyzed channel by channel, or by taking the total number of coincidences obtained over the desired portion of the spectrum. This sytem would be advantageous in studying a level such as the ^{160}Dy 966.4 keV level, when two or more cascades through the same intermediate state can be perturbed; the effects could be studied simultaneously. The main disadvantage would be the lower count rate required by the multi channel analyzer.

By alloying a rare earth source into other rare earths, the effective fields at the nucleus in different lattices can be obtained from a direct comparison of the observed rotations, independent of the lifetime or g-value of the level being used. These fields would be calibrated by using the H_{eff} measured by NMR with the measurement obtained when the source is alloyed into the element to which it decays. In particular, the present experiment should be repeated with the source alloyed into dysprosium metal, to check the assumption that the effective field in an alloy depends on the impurity element rather than on the host. If this assumption proves to be correct, the huge internal fields in the ferromagnetic rare earths would not be available for studying rotations of short-lived states in elements other than the rare earths them-

selves.

Once the effective fields are known, lifetimes measured directly or obtained from B(E2) values should make possible the determination of the g-values of several other short-lived states in the rare earths.

The work presented in this thesis should not be regarded as complete, but as the first step in an interesting sequence of experiments.

REFERENCES

Behrendt, D. R., Legvold, S., and Spedding, F.H. 1958 Phys. Rev. 109 - 1544.

Greiner, W. 1966 - Nuc. Phys. 80 # 2 - 417.

Gschneider, K. A. 1961 - Rare Earth Alloys (Van Nostrand, Toronto).

Hegland, D.E., Legvold, S., and Spedding, F.H. 1963 Phys. Rev. 113 - 158.

Kasuya, T. 1956. Prog. Theo. Phys. 16 - 45.

Kobayaski, S., Sano, N., and Itoh, J. 1966. J. P. Soc. Jap. 21 - 1456.

Koehler, W. C. 1965. Jour. Appl. Phys. 36 - 1078.

Kondo , J. 1961. J. P. Soc. Jap. 16 - 1690.

Kundig, W. 1961. Helv. Phys. Acta 34-125.

Marshall, W. 1961. Phys. Rev. 110 - 1280.

Rhyne, J. J. and Clark, A. E. 1967. Jour. Appl. Phys. 38 - 1379,

Ruderman, M. A.,and Kittel, C. 1954. Phys. Rev. 96 - 99.

Steffen, R. M., and Frauenfelder, H. - chapters in Alpha-, Beta-, and Gamma-Ray Spectroscopy 1966 (North Holland Amsterdam - edited by K. Seigbahn) and in Perturbed Angular Correlations 1964 (North Holland, Amsterdam - edited by E. Karlsson, E. Matthias, and K. Seigbahn.

Watson, R. E. and Freeman, A. J. 1961. Phys. Rev. 123 - 2027.

Yates, M.J.L. - appendix to Perturbed Angular Correlations 1964 (North Holland, Amsterdam - edited by E. Karlsson, E. Matthias, and K. Siegbahn).

Yoshizawa, Y., Elbek, B., Hereskind, B., and Olesen, M. C. 1965. Nuc. Phys. 73 - 273.

Yosida, K. 1957. Phys. Rev. 106 - 893.

Yosida, K. - chapter 5 in Vol. IV, Progress in Low Temperature Physics 1964 (North Holland, Amsterdam - edited by Gorten).

General References

Chikazumi, S. - Physics of Magnetism 1964 (Wiley, New York).

Nuclear Data Sheets (National Academy of Sciences, - National Research Council, Washington, D.C.).

Preston, M. A.-Physics of the Nucleus, 1962. (Addison-Wesley, Reading, Mass.)

Rado, G. T. and Suhl, H. - Magnetism Vol. IIA 1965 (Academic Press, New York).